Similarities on the mode of action of the terpenoids citral and farnesene in *Arabidopsis* seedlings involve interactions with DNA binding proteins

López-González D[1], Graña E[1], Teijeira M[2,3], Verdeguer M[4], Reigosa MJ[1], Sánchez-Moreiras AM[1*], Araniti F[5*]

[1]Universidade de Vigo. Departamento de Bioloxía Vexetal e Ciencia do Solo, Facultade de Bioloxía. Campus Lagoas-Marcosende s/n, 36310 Vigo, Spain;

[2] Universidade de Vigo, Departamento de Química Orgánica, Facultade de Química, 36310 Vigo, Spain; qomaca@uvigo.es

[3] Instituto de Investigación Sanitaria Galicia Sur, Hospital Álvaro Cunqueiro, 36213 Vigo, Spain

[4]Instituto Agroforestal Mediterráneo (IAM), Universitat Politècnica de València, Camino de Vera s/n, 46022 Valencia, Spain

[5]Dipartamento di Science Agrarie e Ambientali – Produzione, Territorio, Agroenergia, Università Statale di Milano, Via Celoria n º2, 20133 Milano, Italy

Corresponding Authors:

F. Araniti fabrizio.araniti@unimi.it,

A.M. Sánchez-Moreiras adela@uvigo.es

Abstract

The sesquiterpene farnesene and the monoterpene citral are phytotoxic natural compounds characterized by a high similarity in macroscopic effects, suggesting an equal or similar mechanism of action when assayed at IC_{50} concentration. In the present study, a short-time experiment (24 and 48 h) using an imaging spectrofluorometer allowed us to monitor the *in-vivo* effects of the two molecules, highlighting that both terpenoids were similarly affecting all PSII parameters, even when the effects of citral were quicker in appearing than those of farnesene. The multivariate, univariate, and pathway analyses, carried out on untargeted-metabolomic data, confirmed a clear separation of the plant metabolome in response to the two treatments, whereas similarity in the affected pathways was observed. The main metabolites affected were amino acids and polyamine, which significantly accumulated in response to both treatments. On the contrary, a reduction in sugar content (i.e. glucose and sucrose) was observed. Finally, the *in-silico* studies demonstrated a similar mechanism of action for both molecules by interacting with DNA binding proteins, although differences concerning the affinity with the proteins with which they could potentially interact were also highlighted. Despite the similarities in macroscopic effects of these two molecules, the metabolomic and *in-silico* data suggest that both terpenoids share a similar but not equal mechanism of action and that the similar effects observed on the photosynthetic machinery are more imputable to a side effect of molecules-induced oxidative stress.

Keywords: *Arabidopsis thaliana*, chlorophyll *a* fluorescence, *in silico* studies, metabolomics, molecular docking, natural compounds.

INTRODUCTION

Weeds are one of the main problems farmers face, as they compete with crops for edaphic resources, causing a loss in crop yield and quality (Hachisu, 2021). The quickest and cheapest solution for many farmers is the use of synthetic herbicides, a common practice for the last 70 years (Duke et al., 2018). However, these compounds have numerous adverse effects, such as being harmful to the environment or human health, and the emergence of resistant weeds due to their indiscriminate use. Only one herbicide with a new MOA (cyclopyrimorate) has been introduced on the market since 1980, and one is close to being introduced (tetflupyrolimet) (Duke and Dayan, 2021), but no more herbicides with new modes of action (MOAs) have been discovered in the last 30-40 years. This is why searching for new molecules with a potential bioherbicidal capacity that presents new molecular targets is necessary.

Natural compounds are a source of new pesticides with potential new modes of action, different from those of current herbicides, which could help to tackle the problem of weed's resistance (Duke et al., 2018). In addition, it is possible that a natural compound with an already known MOA is effective against a weed with resistance to that MOA, as the structural diversity of natural compounds allows them to bind to the target site differently from the conventional herbicide and become effective (Duke and Dayan 2021). Moreover, many natural compounds have been found to show more than one molecular target site and more than one MOA, which makes them more effective in avoiding weed resistance (Duke et al., 2020; Gressel 2020). For example, the natural compound sorgoleone inhibits the D2 protein in the photosystem II (PSII) and also inhibits the enzyme 4-hydroxyphenylpyruvate dioxygenase (involved in PSII plastoquinone synthesis), and linarin inhibits seed respiration, germination, root and hair growth and the donor side of PSII (Gressel 2020).

Recently, the use of *-omics* techniques and molecular, biochemical and physiological techniques has significantly impacted the study of the effect of natural compounds on plant metabolism (Araniti et al., 2020). Of all the omics, metabolomics is the one that explains the phenotype by correlating it with changes in the metabolome. Studying the metabolome and its changes in response to bioactive compounds can generate important information on the MOA of natural compounds (Aliferis, 2020). For example, Trenkamp et al. (2009) used GC-MS to observe the effects of various herbicides (glufosinate, glyphosate, sulcotrione, etc.) on the metabolome of *A. thaliana*. Moreover, recently, metabolomics has begun to be widely used in studying the stresses and mechanisms of action of natural molecules with potential bioherbicide activity (Shualev et al, 2008; Misra et al., 2020).

Among these specialized metabolites with potential bioherbicide activities, terpenoids are one of the classes characterized by a significant biological activity widely studied in the last years (Verdeguer et al., 2020).

The monoterpene citral, firstly characterized in the essential oil of *Citrus aurantiifolia*, is an interesting terpenoid with strongly demonstrated phytotoxicity (Chaimovitsh et al., 2012; Graña et al., 2013b). Vaughn and Spencer (1993) were the first to show that the saturation of desiccator flasks with citral vapours induced a 32, 80 and 96% inhibition of germination of maize, soybean and cucumber, respectively. When used in solution, it was phytotoxic for lettuce, barley, wild oat, ribwort, redroot pigweed and barnyard grass and caused oxidative damage to *A. thaliana* (Graña et al., 2013a). This compound also induced the disorganization of microtubules on wheat and *A. thaliana* (Chaimovitsh et al., 2011) and reduced cell division in *A. thaliana* roots, causing disorganization of root cells and altering the hormonal balance of auxin and ethylene in *Arabidopsis* seedlings (Graña et al., 2013b). Also, it caused

a decrease in the mitotic index in onion plants (Fagodia et al., 2017). Graña et al. (2020) reported that with just one-hour exposition to citral, *A. thaliana* seedlings showed 9000 genes strongly down-regulated in roots and 5500 in shoots. Moreover, *in silico* studies demonstrated that citral isomers (neral and geranial) can interact with many single-stranded DNA-binding proteins (SSBPs), causing a direct inhibition of gene transcription in *Arabidopsis* treated seedlings (Graña et al., 2020).

Farnesene (Fig. 1) is a widely distributed sesquiterpene involved in both plant- and insect-communication (Vourinen et al., 2003), which has also shown phytotoxic potential in altering the root growth of *A. thaliana* seedlings (Araniti et al., 2013).

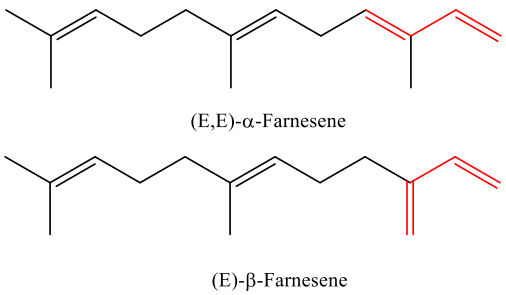

Figure 1. Farnesene's alpha (up) and beta (down) stereoisomers. The double bond position that differentiates the stereoisomers is shown in red.

Farnesen causes an increase in auxin and ethylene levels and stimulates oxidative damage through the production of NO, H_2O_2 and O_2^-, causing disruption of mitotic and cortical microtubules and inducing ultra-structural cell malformations that alter root growth of *A. thaliana* and remember those of citral (Araniti et al., 2016). Later, Araniti et al. (2017a) demonstrated that the microtubule disruption was a consequence of an altered auxin distribution caused by a farnesene-induced downregulation of the expression of all the auxin polar transport PIN proteins, accompanied by a degradation of the proteins PIN4 and PIN7, at the level of the quiescent center. Although the MOA of farnesene has not been studied so profoundly as citral, many of the effects observed for both compounds are highly similar (morphological alterations in the root, malfunction of microtubules, altered auxin balance, etc.), suggesting the possibility of shared action pathways for both terpenoids. Moreover, a visual comparison of neral and farnesene reveals a high structural similarity since the 1,5-octadienyl chain is present in both structures, which could determine their mode of action. Furthermore, there are already synthetic herbicides with a different chemical structure that affect the same molecular target, e.g., glyphosate and imazaquin (Gaines et al., 2020), which suggest that even with different chemical structures two natural compounds could share one or more target sites of action. Citral and farnesene are Generally Recognized

as Safe (GRAS) food additives by the US Food and Drug Administration. Moreover, it was demonstrated that farnesene acts as a neuroprotective agent against hydrogen peroxide-induced neurotoxicity *in-vitro* and could be used as an antioxidant compound resource that may have applications in the food and drug industries (Çelik et al., 2014).

Therefore, independent metabolomic studies of *A. thaliana* seedlings treated at two different times (24 and 48 h) with the IC_{50} of citral and farnesene were done, together with *in silico* studies of the interaction of farnesene with the single-stranded DNA-binding proteins (SSBPs) and the comparison of the binding sites of farnesene with those previously found for citral (Graña et al., 2020). Farnesene is a mixture of six unsaturated sequiterpenes, among which the alpha and beta stereoisomers differ in the arrangement of the conjugated double bonds (Fig. 1). The (3E,6E)-3,7,11-trimethyldodeca-1,3,6,10-tetraene, namely (E,E)-α-farnesene isomer, is the most widespread in nature. However, there can be more than four alpha geometric stereoisomers in two of its three internal double bonds. Furthermore, the (E,E)-α-farnesene structure has two methylene bridges that provide conformational flexibility. To study the putative molecular mechanisms of farnesene as a potential bioherbicide and to compare these results to those previously found for citral (Graña et al., 2020), its binding affinities to different transcription factors (AtWHY-2, ANAC and SHR-SCR complex) were calculated with ICM docking approaches.

In addition, parameters related to the PSII photosynthetic performance of plants treated with citral and farnesene were also studied in a short-term experiment on *Arabidopsis* seedlings at the same measuring times as the metabolomics study to investigate the mechanism of action of these two specialised metabolites and to compare whether they have similar modes of action on the photosynthetic process. A sensitive imaging fluorometer technique was adopted as a fast-screening method to effectively compare *in-vivo* the effects of these two terpenoids on seedling performance.

MATERIALS AND METHODS

Plants growth conditions

Arabidopsis thaliana (L.) Heynh. ecotype Columbia (Col-0) seeds were sterilised and vernalized as previously described by Araniti et al. (2016) and sown (24 seeds per replicate) in square Petri dishes (100 x 150 mm) filled with plant agar (0.8% w/v) enriched with micro- and macro-nutrients (basal salt-medium Murashige-Skoog, Sigma-Aldrich) and supplemented with 1% sucrose (pH 6.0). The plates were placed, vertically for metabolomic studies or horizontally for chlorophyll *a* fluorescence measurements, in a growth chamber at 22 ± 2 °C, 55% relative humidity and a short-day photoperiod with 8 daylight

hours (75 μmol $m^{-2}s^{-1}$) and 16 h darkness. Plants were left to grow for 14 days. After this time, 4 mL of the IC_{50} (323 μM, Araniti et al., 2013) of farnesene (Sigma-Aldrich) or the IC_{50} (194 μM, Graña et al., 2013b) of citral (Sigma-Aldrich) were added to each plate. The compounds were diluted in 0.1% ethanol as solvent (control plates included 0.1% EtOH, too). Then, plates were incubated horizontally for 24 and 48 h. Although previous gene expression and *in-silico* studies were done with citral for 1 to 24 h (Graña et al., 2020), the measuring times used in this work for comparison of citral and farnesene effects were set up at 24 and 48 h to allow protein codification, enzymatic reactions and metabolites' synthesis as a consequence of these first observed effects for citral.

Chlorophyll *a* fluorescence measurements

The imaging fluorometer was used during the experiments as a screening tool since the primary phytotoxic effects of a specific toxin can be quickly monitored *in-vivo* on the same plant, and the effects are visible even before macroscopic alterations such as chlorosis, necrosis or growth reductions can be detected (Sánchez-Moreiras et al., 2020). The chlorophyll *a* fluorescence emitted by plants (four seedlings per treatment and time) was determined as described by Graña et al. (2013b) with a Maxi-Imaging-PAM fluorometer (Walz, Effeltrich, Germany) after 0, 24 and 48 hours of treatment with IC_{50} of farnesene and citral. This apparatus gives all the parameters related to the measurement of chlorophyll *a* fluorescence, and takes pictures of this fluorescence to obtain a view of the photosynthetic activity of the entire plant and its spatio-temporal variations over time (Martínez- Peñalver et al., 2011; Sánchez-Moreiras et al., 2020). The plants were kept in darkness for 10 min to open all the reaction centers. After this time, seedlings were successively illuminated at 0.5 $\mu mol \cdot m^{-2} \cdot s^{-1}$ to measure the initial fluorescence (F_0). Then a saturating pulse of 2700 $\mu mol \cdot m^{-2} \cdot s^{-1}$ was used to measure the maximum fluorescence of dark-adapted seedlings (F*m*). After five minutes of actinic illumination at 120 $\mu mol \cdot m^{-2} \cdot s^{-1}$ (with measurement of the corresponding fluorescence, F_s), samples received 20 s of 800-ms saturating pulses of 200 $\mu mol \cdot m^{-2} \cdot s^{-1}$ to assess the maximum fluorescence of light-adapted leaves (F*m*'). These values were used to calculate the parameters used for comparisons between treatments: maximum quantum efficiency of dark-adapted photosystem II (F*v*/F*m*); quantum efficiency of photosystem II (Φ_{II}); energy dissipation in the form of heat (Φ_{NPQ}); non-regulated energy dissipation (Φ_{NO}, fluorescence emission); and the estimated electron transport rate (ETR) (Kramer et al., 2004; Klughammer and Schreiber, 2008). The photosynthetic response was monitored for 5 min, and fifteen measurements were obtained for each parameter.

Extraction, identification and quantification of primary metabolites

Extraction, derivatisation, identification, and quantification of metabolites from *Arabidopsis* shoots treated for 24 and 48 h with citral or farnesene (IC_{50}) were performed, as reported by Lisec et al. (2006). The derivatised extracts were injected into a gas chromatograph apparatus (Thermo Fisher G-Trace 1310) coupled to a single quadrupole mass spectrometer (ISQ LT). Samples chromatographic separation was achieved using a capillary column TG-5MS 30 m×0.25 mm×0.25 µm and helium (6.0) as carrier gas. The injector and source were settled at 250 °C and 260 °C, respectively. One µL of the sample was injected in splitless mode with a flow of 1 mL min^{-1}. The programmed temperature was settled as follows: isothermal at 70 °C for 5 min followed by a 5 °C/ min ramp to 350 °C and final heating at 330 °C for 5 min. Mass spectra were recorded in electronic impact (EI) mode at 70 eV, scanning at 45–600 m/z range. Chromatographic alignment, deconvolution, intensity extraction and peaks annotation were carried out using the open source software MS-DIAL. The average peak width of 20 scans and a minimum peak height of 1000 amplitudes was applied for peak detection. The sigma window value was 0.5 and EI spectra cut-off of 10 amplitudes was implemented for deconvolution. For peaks identification, the retention time tolerance was settled at 0.5 min, the m/z tolerance at 0.5 Da, the EI similarity cut-off was 70%, and the identification score cut-off was 70%. In the alignment parameters setting process the retention time tolerance was settled to 0.075 min. Metabolites annotation was achieved using an in-house library built with publicly available MS spectra, as Misra (2019) reported.

Metabolites identification was made following the metabolomics standards initiative guidelines (MSI) for metabolite identification (Sansone et al., 2007). In particular, features were annotated at Level 2 [identification based on the spectral database (match factor >70%)] and Level 3 [identification based on the spectral database (match factor >70%)]. Relative metabolites normalization was based on an internal standard (ribitol at 0.02 mg mL^{-1}), added during the extraction process (Lisec et al., 2006).

***In silico* studies**

Molecular modelling studies

Flexible ICM (Internal Coordinate Mechanics software) docking was used to optimize the internal coordinates of the farnesene located in the protein pocket. Previously, conformational analysis was performed outside the protein pocket, and low-energy conformations were used as initial geometries for docking. Ligand binding modes were scored according to the farnesene-target complex results and ranked using the full ICM scoring function. A low ICM score suggests favourable ligand-protein binding

affinity. The scoring function was calculated as the weighted sum of the following parameters (Shapira et al., 1999): internal force-field energy of the ligand, entropy loss of the ligand between bound and unbound states, ligand-receptor hydrogen bond interactions, polar and non-polar solvation energy differences between bound and unbound states, electrostatic energy, hydrophobic energy, and hydrogen bond donor or acceptor desolvation.

Receptor Preparation

All proteins were prepared using the default ICM (Internal Coordinate Mechanics) settings (Abagyan and Totrov, 1994). The Protein Data Bank (PDB) crystal structures of AtWHY-2 (PDB code 4KOP: 1.8Å resolution); ANAC (PDB code: 1ut7: 1.9 Å resolution); and SHR-SCR complex (PDB code 5b3g: 2 Å resolution) proteins from *Arabidopsis thaliana* were converted to ICM objects.

Ligand preparation

α-Farnesene structure (PubChem CID 5281516) and citral (PubChem CID 643779) were imported into ICM, converted to 3D structure, and all conformers were calculated, i.e. to generate 3D series of conformers for both ligands, a maximum number of conformations of 30, an effort value of 10 and a thoroughness of 10 were calculated. Farnesene and citral molecules were first subjected to conformational analysis outside the protein pocket using the MMFF force field. Low energy conformations were collected and used as starting geometries for protein-ligand docking.

Molecular docking

α-Farnesene and citral were placed into WHY-1, WHY-2, WHY-3 proteins from the Whirly family (Protein Data Bank, PDB code 4KOO: 1.9 Å resolution; 4KOP: 1.8 Å resolution; 4KOQ 1.9 Å resolution); ANAC from the NAC family (PDB code: 1ut7: 1.9 Å resolution); SHR-SCR complex from the GRAS family (PDB code 5b3g: 2 Å resolution), and MYC2 tetrameric from the bHLH family (PDB code 5GNJ: Resolution: 2.7 Å resolution) from *A. thaliana,* and docking poses were scored by scoring functions according to their most energetically favourable protein binding conformation, using ICM flexible docking method (Abagyan et al., 1994).

Statistical analysis

A completely randomised design with four replicates was applied in all the experiments. Chlorophyll fluorescence parameters were analysed through one-way ANOVA using Tukey's test as

post-hoc ($p \leq 0.05$). Metabolite concentrations were checked for integrity, and missing values were replaced by a small positive value (half of the minimum positive number detected in the data). Data were successively normalised by a reference sample (ribitol), transformed through "Log normalisation" and scaled through Auto-Scaling. Data were then classified through unsupervised Principal Component Analysis (PCA) to get the score plot (to visualise group discrimination) and the loadings plot (to identify metabolites contributing to groups separation). The data were further analysed through the supervised Partial least-squares discriminant analysis (PLS-DA). Features selection, with the highest discriminatory power, was based on their variable importance in projection (VIP) score > 1. To avoid overfitting, the PLS-DA model was validated using Q2 as a performance measure, the 10-fold cross-validation and setting in the permutation test a permutation number of 20 (see figures reported in Supplementary Table S1-PLSDA loadings).

Data were then analysed through the univariate analysis one-way ANOVA using the LSD test as post-hoc ($P \leq 0.05$) to highlight statistical differences among single metabolites and treatments. A false discovery rate was applied to the nominal *p*-values as a control for false-positive findings. All the features significantly affected by the treatments (in the ANOVA test) were presented as a heatmap and clusterised using the Euclidean method for distance measurement and the Ward algorithm for group clusterisation. Further, a Student's *t*-test analysis ($P \leq 0.05$) was carried out for each time of exposure (24hr and 48hr) to identify potentially different metabolites affected by the treatments.

Finally, a pathway analysis was performed with MetPA, a web-based tool that combines results from pathway enrichment analysis and topology analysis, which allowed the evaluation of the possible biological impacts on the perturbed pathways (Araniti et al., 2017b). All the metabolomics analyses were carried out using Metaboanalyst 3.0 (Xia et al., 2015). All the raw and analysed metabolomic data are reported in supplementary material, Table S1.

RESULTS

Many similarities, but also some differences, could be detected among citral and farnesene treatments when looking at the metabolomic variations in *Arabidopsis* seedlings treated with both compounds after the same measuring times than those of fluorescence emission. In order to assess the influence of the treatments on overall metabolites, raw data were analyzed through principal component analysis (PCA) for the 67 compounds identified by GC-MS analyses (Table 1).

Table 1. The annotated and relatively quantified chemical compounds significantly affected after the exposition to farnesene (323 µM) and citral (194 µM) for 24 or 48 h.

Molecules	F24	F48	C24	C48	
	t.stat				
Beta-Alanine	//	**-3.531**	//	**-8.804**	**Aminoacids**
GABA	//	**-4.744**	**-19.11**	**-7.152**	
Glycine	//	13.82	//	6.843	
L-Alanine	//	//	**-5.845**	**-5.041**	
L-Asparagine	//	//	//	**-6.202**	
L-Aspartic acid	//	//	23.71	14.18	
L-Glutamic acid	//	**-3.732**	//	7.845	
L-Glutamine	//	**-7.970**	**-6.360**	**-10.39**	
L-Lysine	**-12.65**	**-5.453**	**-10.33**	**-4.094**	
L-Proline	//	//	**-4.866**	**-14.09**	
L-Serine	**-5.795**	**-7.698**	**-7.989**	**-18.65**	
L-Threonine	//	**-9.210**	**-8.083**	**-6.791**	
Pyroglutamic acid	//	//	//	**-3.410**	**Amino acid derivative**
Cadaverine	**-4.076**	**-8.558**	**-18.45**	**-17.07**	**Polyamines**
Citrulline	**-4.368**	**-5.678**	//	**-4.341**	
Ornithine	//	**-3.668**	**-6.984**	**-4.671**	
Putrescine	**-13.06**	**-19.95**	**-11.96**	**-13.48**	
2-Keto-D-gluconic acid	//	**-6.651**	**//**	**-6.829**	**Organic acids**
Citric acid	**-4.684**	//	//	5.731	
Oxalic acid	//	//	//	7.516	
Oxoglutaric acid	//	//	//	10.85	
Glutaric acid	//	//	**-6.247**	//	
Glyceric acid	9.608	5.935	//	6.549	
Glycolic acid	//	//	**-4.234**	//	
Pyruvic acid	//	4.737	3.193	8.272	
Propionic acid	//	//	**-5.894**	//	
Succinic acid	//	6.342	5.724	6.434	
Threonic acid	//	**-8.160**	**-3.378**	**-10.99**	
Allose	//	**-10.99**	//	//	**Sugars**
Alpha-Lactose	**-16.84**	**-9.342**	**-17.56**	**-11.09**	
Erythrose	//	//	5.247	3.395	
D-Glucose	//	//	//	3.802	
Sucrose	8.780	6.320	5.070	5.239	
Turanose	3.836	//	//	4.291	
Myoinositol	//	//	**-5.127**	//	**Sugar alcohol**
Sinapic acid	//	//	5.856	6.918	**Phenolic acids**
Benzoic acid	//	21.50	//	22.61	
Palmitelaidic acid	//	**-5.695**	9.301	//	**Fatty acids**
Dodecanoic acid	//	//	44.97	**-4.357**	
Decanoic acid	//	//	//	**-13.08**	
Adipic acid	//	6.782	//	2.929	
3-Indoleacetonitrile	//	//	11.44	6.593	**Miscellaneous**
Phosphoric acid	**-6.333**	**-11.65**	**-7.913**	**-6.886**	
Urea	11.08	3.876	8.733	6.069	
N-Alpha-acetyllysine	**-4.353**	**-10.16**	**-10.34**	**-14.26**	

Important features selected by t-tests with threshold $p \leq 0.05$. Negative t-stat values indicate up-accumulated metabolites, whereas positive t-stat indicates down-accumulated metabolites. //: Not Significant features. Data are expressed in nanograms/100 mg of fresh plant material. N=4.

The score plot of the unsupervised PCA (Fig. 2a) highlights the separation between control and treatments. The grouping observed during PCA analysis was further confirmed by cluster analysis (Fig. 2d), which pointed out the formation of two main separated groups (control and treatments), being citral and farnesene grouped in the same cluster branch at the higher level and in separated units at a lower level (Control, Farnesene and Citral) (Fig. 2d). The supervised PLS-DA analysis (Fig. 2b) confirmed the separation, previously observed with the PCA, characterized by three separated groups (control, citral and farnesene), which were distributed in three different quadrants. Interestingly, while both farnesene samples (24 and 48 h) were grouped, citral treatments were separated, indicating a stronger effect of citral when increasing the time of exposure (Fig. 2a). The separation was achieved by virtue of the first two principal components (PCs) PC1 *vs* PC2, which explained a total variance of 45%. PC1 explained the highest variance (31%), while PC2 explained the 14% of the total variance. The PCA loading plot highlighted that PC1 was dominated by putrescine, N-α-acetyllysine, cadaverine, L-threonine, serine, sucrose and glyceric acid, whereas PC2 was dominated by glutamic, fumaric, citric, malic, decanoic and propionic acids, and alanine (supplementary material, Table S1). Moreover, the VIP score analysis pointed out that several sugars, polyamines and amino acids were the classes of compounds mainly contributing to groups discrimination (Fig. 2c). In particular, the treatments with citral induced, at both times of treatment (24 and 48 h), a significant accumulation of phosphoric acid, L-lysine, citrulline, ornithine, putrescine, cadaverine and threonic acid, and a reduction in glucose, pyruvic acid, fructose, urea, sucrose, and glycine (Fig. 2c). A similar trend was also followed by farnesene, which induced increments and decrements of the same metabolites affected by citral even when the differences were less marked (Fig. 2d).

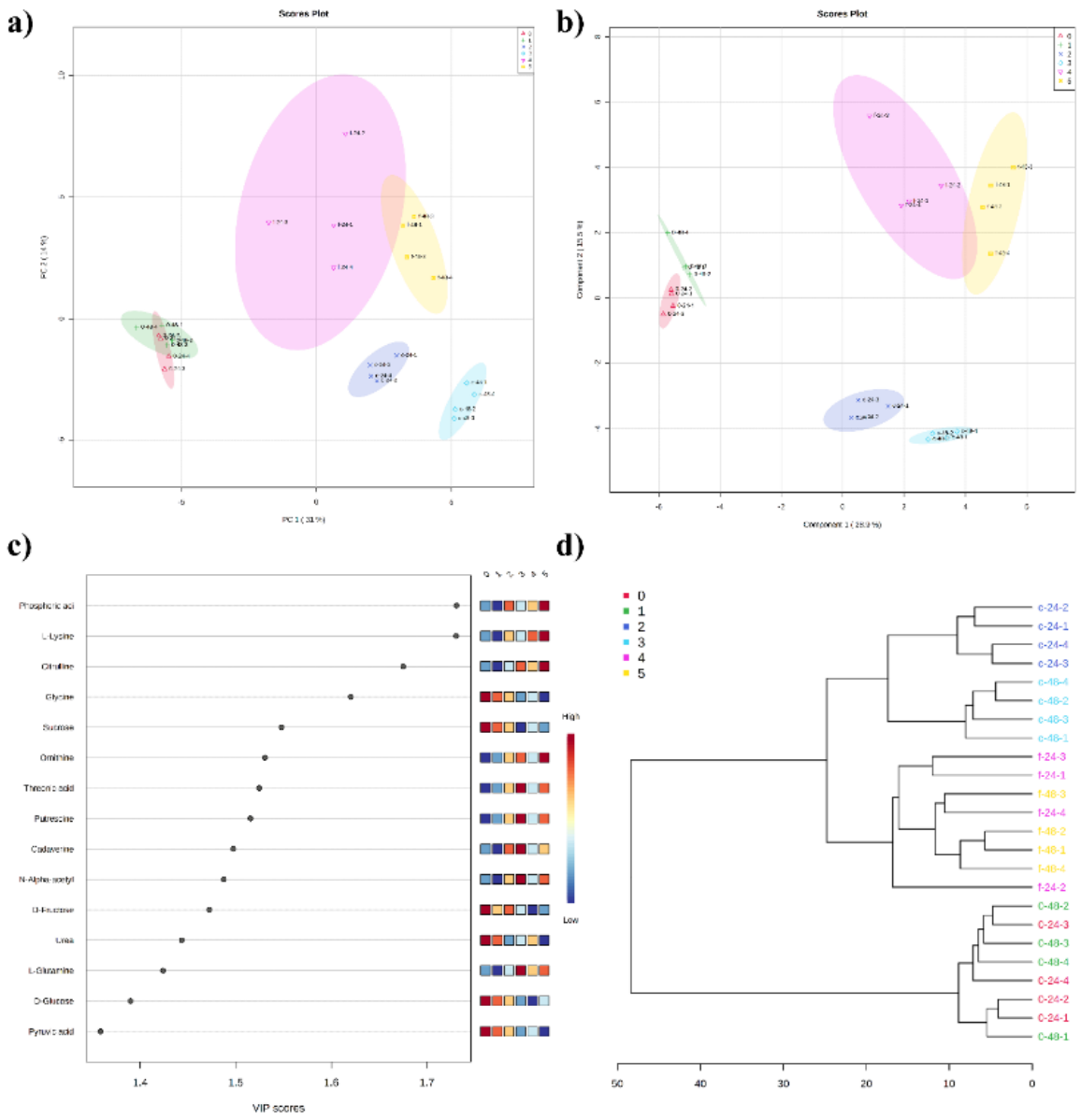

Figure 2. PCA (a), PLS_DA (b-c) and cluster analysis (d) carried on the metabolite identified and quantified after farnesene (323 µM) and citral (194 µM) treatments. a) PCA scores plot between the selected PCs; b) PLS-DA scores plot between the selected PCs, the explained variances of PCA and PLS-DA are shown in brackets; c) Important features identified by PLS-DA. The coloured boxes on the right indicate the relative concentrations of the corresponding metabolite in each group under study; d) Clustering result shown as a dendrogram (distance measure using euclidean, and clustering algorithm using ward. D). 0-24 (0, ▲ or red colour) and 0-48 (1, + or green colour) indicate control replicates after 24 and 48 h, respectively; C-24 (2, X or dark blue) and C-48 (3, ○ or light blue) indicate citral replicates after 24 and 48 h; F-24 (4, ▼ or magenta) and F-48 (5, □ or yellow) indicate farnesene replicates after 24 and 48 h, respectively, respectively. N=4.

The univariate ANOVA analysis revealed that 40 out of the 67 compounds identified were significantly altered among both treatments (supplementary material, Table S1). Those 40 metabolites were reported on a heatmap, which gave an overview of the trend of each metabolite among the treatments and times of exposition (Fig. 3). Finally, a t-test analysis was carried out comparing each treatment at a given time of treatment (24 or 48 h) with its relative control (24 or 48 h) and the results were reported in Table 1. The analysis highlighted that in total 45 metabolites out of 67 were affected by the treatments. In particular, after 24 h, only 28 and 13 metabolites were affected by citral and farnesene respectively, whereas at 48 h, 39 and 26 metabolites were respectively affected. Interestingly, when we compare 24 h treatment of citral with 24 h farnesene, just nine metabolites were found to be commonly affected, while when comparing 48 h citral with 48 h farnesene, there were up to 22 metabolites commonly affected. Notably, most amino acids and polyamines increased their levels between treatments, while sugars decreased, except for alpha lactose and allose, which increased. As for organic and fatty acids and miscellaneous compounds, some of them increased while others decreased, whereas phenolic acid levels were reduced between treatments (Table 1 and supplementary material, Table S1).

Finally, a detailed analysis concerning the pathways affected by farnesene and citral treatments was performed using the metaboanalyst module "MetPa". The pathway analysis of the results allowed identifying treatment impact on plant metabolism. In general, farnesene and citral similarly affected the same pathways after 48 h of treatment, whereas the exposure to both molecules for 24 h highlighted that citral was more rapid than farnesene in affecting those pathways (Table 2). In particular, 20 pathways were significantly affected by citral and farnesene treatments, but only 11 had an impact score higher than 0.20. The three routes with a pathway impact score higher than 0.50 were alanine, aspartate and glutamate metabolism, beta-alanine metabolism, and glycine serine and threonine metabolism, pathways related to amino acid metabolism (Table 2 and supplementary material, Table S1).

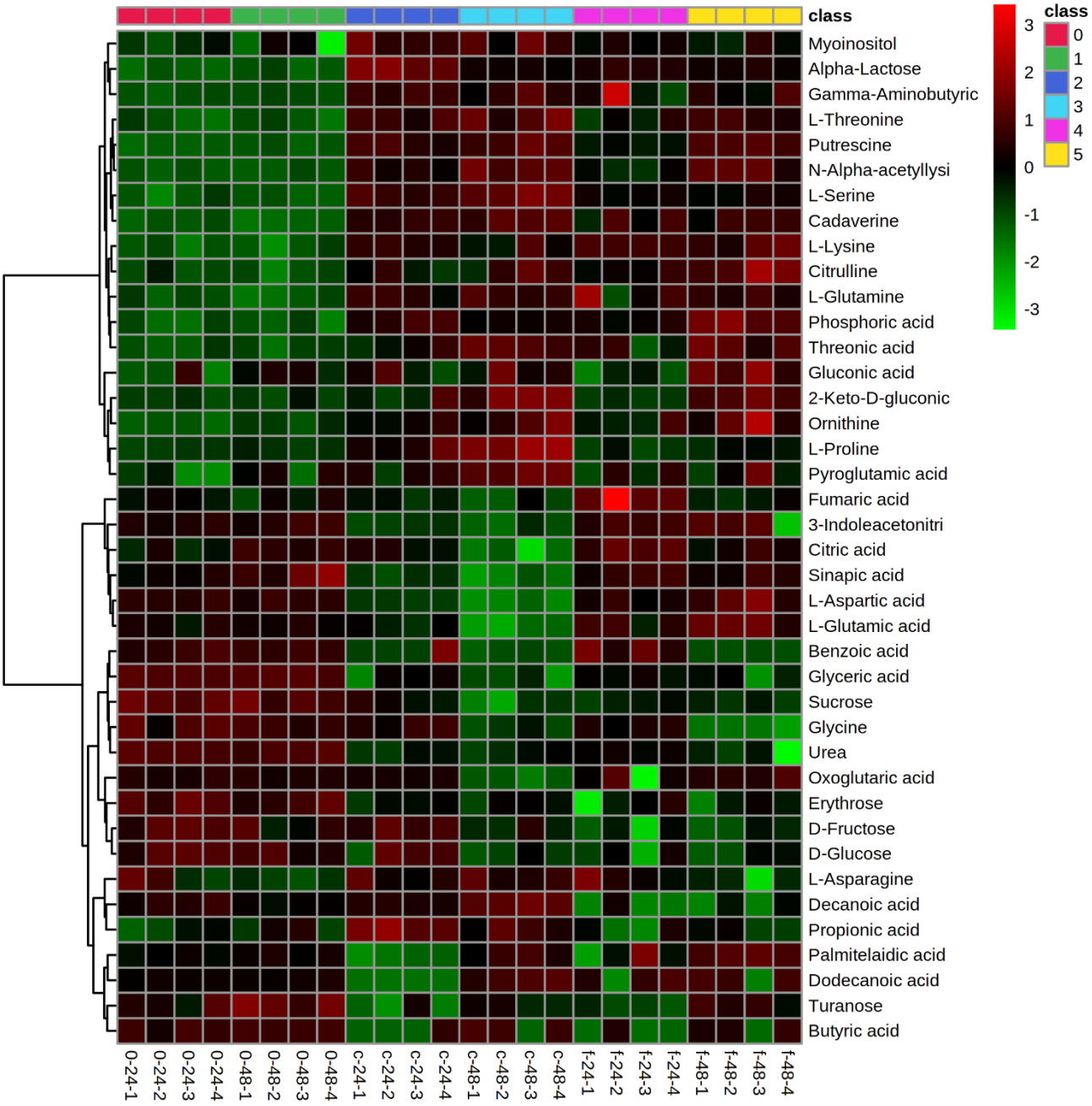

Figure 3. Overlay heat map of the 40 metabolites resulted from the ANOVA test (LSD $p \leq 0.05$ and FDR ≤ 0.05) significantly altered in seedlings exposed to farnesene (323 µM) and citral (194 µM) for 24 and 48 h. Each square represents the effect of farnesene and citral on the amount of every metabolite using a false-colour scale. Dark red or dark green colors respectively indicate an increase or decrease in metabolite content. 0-24 (class 0) and 0-48 (class 1) indicate control replicates after 24 and 48 h, respectively; C-24 (class 2) and C-48 (class 3) indicate citral replicates after 24 and 48 h; F-24 (class 4) and F-48 (class 5) indicate farnesene replicates after 24 and 48 h, respectively. N=4.

Table 2. Results from ingenuity pathway analysis with MetPa carried out on *Arabidopsis* seedlings treated with farnesene (323 μM) and citral (194 μM) for 24 and 48 h.

Pathways	Total Cmpd	Hits	Farnesene 24		Farnesene 48		Citral 24		Citral 48		Impact
			Raw p	-LOG(p)	Raw p	-LOG(p)	Raw p	-LOG(p)	Raw p	-LOG(p)	
Alanine aspartate and glutamate metabolism	22	10	//	//	0.0005	75.981	1.04E-01	11.472	7.17E-03	14.149	0.87
beta-Alanine metabolism	12	2	//	//	0.0046	53.719	//	//	1.44E-04	18.054	0.54
Glycine serine and threonine metabolism	30	5	0.0022	6.1010	2.41E-01	10.631	1.97E-04	15.442	4.79E-03	14.551	0.53
Galactose metabolism	26	6	1.08E-02	11.432	0.0001	91.322	1.35E-02	13.517	0.0001	8.9770	0.47
Arginine and proline metabolism	38	10	7.16E-01	95.446	1.74E-01	10.959	8.52E-05	18.581	1.23E-05	18.216	0.41
Citrate cycle (TCA cycle)	20	6	//	//	2.86E-01	10.462	0.0115	44.682	1.20E-02	13.629	0.28
Glyoxylate and dicarboxylate metabolism	17	4	0.0307	34.849	0.0104	4.5700	0.0050	52.996	0.0010	69.274	0.27
Inositol phosphate metabolism	24	1	0.0136	43.009	//	//	0.0022	61.361	//	//	0.25
Tryptophan metabolism	27	1	//	//	//	//	2.68E-02	10.527	0.0006	74.437	0.21
Pantothenate and CoA biosynthesis	14	3	//	//	1.11E-02	11.405	//	//	2.24E-02	13.010	0.20
Pyruvate metabolism	21	3	//	//	0.0002	85.275	//	//	0.036685	33.054	0.20
Methane metabolism	11	2	9.04E-02	11.614	3.06E-02	12.699	4.68E-01	99.692	1.01E-03	16.104	0.17
Glycolysis or Gluconeogenesis	25	2	//	//	0.0007	72.245	//	//	0.0128	43.602	0.11
Aminoacyl-tRNA biosynthesis	67	11	//	//	1.61E-01	11.035	2.60E-03	15.163	8.41E-05	18.594	0.09
Starch and sucrose metabolism	30	3	0.0019	62.883	0.0043	54.468	0.0014	65.971	0.0027	59.048	0.09
Glutathione metabolism	26	5	0.0025	59.886	5.41E-03	14.431	5.26E-02	12.156	4.32E-04	16.956	0.09
Lysine biosynthesis	10	2	3.47E-01	10.270	0.0027	59.141	1.77E-03	15.546	6.93E-02	11.879	0.07
Phenylpropanoid biosynthesis	45	1	0.0469	30.595	//	//	0.0011	68.164	0.0005	7.7030	0.04
Carbon fixation in photosynthetic organisms	21	4	//	//	0.0027	59.043	0.0002	83.857	7.46E-02	11.807	0.03
Valine leucine and isoleucine biosynthesis	26	3	//	//	0.0001	9.1770	0.0005	75.641	8.20E-02	11.711	0.02
Purine metabolism	61	2	0.0032	5.7450	0.0006	74.136	0.0001	9.1350	7.63E-01	94.807	0.01

Total Cmpd: the total number of compounds in the pathway; Hits: is the matched number from the uploaded data; P value: is the original *p* value calculated from the enrichment analysis; Impact: is the pathway impact value calculated from pathway topology analysis. //: not significantly impacted pathways. N=4.

If we look at the results obtained from the measurement of chlorophyll *a* fluorescence, all parameters related to this measurement were affected by both treatments, IC_{50} farnesene and citral (Fig. 4), at the two treatment times of exposure (24 and 48 h). Farnesene and citral significantly reduced the photochemical quenching (Φ_{II}). The Φ_{II} value in control was 4.48 A.U. after 48 h, while in citral and farnesene treatments the values were 1.75 and 2.57 A.U., respectively. Both compounds caused a significant increase in heat energy dissipation (Φ_{NPQ}, from 2.46 A.U. in control to 6.04 and 4.02 A.U. in citral and farnesene treatments) and non-regulated energy emission as fluorescence (Φ_{NO}, from 5.06 A.U. in control to 7.69 and 7.29 A.U. in citral and farnesene respectively). However, farnesene-treated plants were most able to maintain high levels of regulated energy emission (Φ_{NPQ}) than citral-treated plants after 48 h of treatment

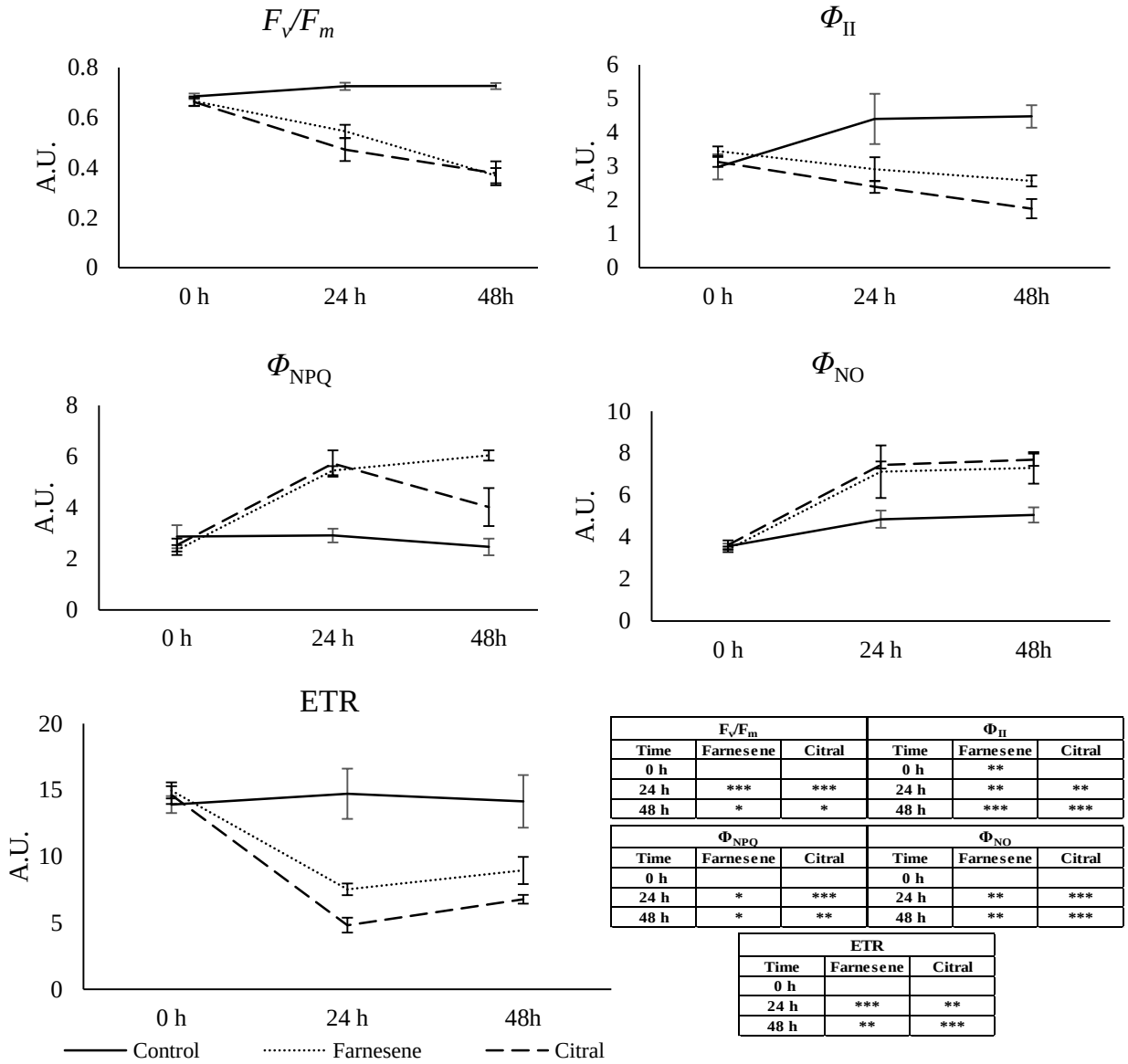

F_v/F_m			Φ_{II}		
Time	Farnesene	Citral	Time	Farnesene	Citral
0 h			0 h	**	
24 h	***	***	24 h	**	**
48 h	*	*	48 h	***	***

Φ_{NPQ}			Φ_{NO}		
Time	Farnesene	Citral	Time	Farnesene	Citral
0 h			0 h		
24 h	*	***	24 h	**	***
48 h	*	**	48 h	**	***

ETR		
Time	Farnesene	Citral
0 h		
24 h	***	**
48 h	**	***

Figure 4. Values of the maximum quantum efficiency of dark-adapted PSII (F_v/F_m), the effective photochemical quantum yield of the light adapted PSII Φ_{II}, the quantum yield of light induced nonphotochemical quenching Φ_{NPQ} (mainly heat), the chlorophyll fluorescence Φ_{NO},

and the apparent electron transport rate (ETR) in *Arabidopsis* seedlings treated at 0, 24 and 48 h with IC_{50} farnesene and IC_{50} citral. Control treatment represents untreated seedlings. Asterisks indicate significant * $p < 0.05$; very significant ** $p < 0.01$; and highly significant *** $p < 0.001$ differences when compared to the control. AU = Arbitrary Units. N = 4.

The Φ_{NO} images (Fig. 5) show how both treatments can similarly damage the cells close to the vascular bundles already 24 h after the treatment, and this effect was stronger with both compounds after 48 h of treatment. The electron transport rate (ETR) was also significantly reduced in both treatments at both times. At 48 h, there was a decrease from 14.15 A.U. in control to 6.78 and 8.95 A.U. in citral and farnesene, respectively. Finally, the maximum efficiency of PSII dark-adapted system (F_v/F_m) was significantly reduced, from 0.73 A.U. in control to 0.38 and 0.37 A.U. in citral and farnesene, respectively, after 48 h of treatment. As shown in the F_v/F_m image (Fig. 5), this parameter was reduced in the center of the rosette at 24 h of treatment. Successively, this reduction extended to the rest of the seedling shoot after 48 h of treatment.

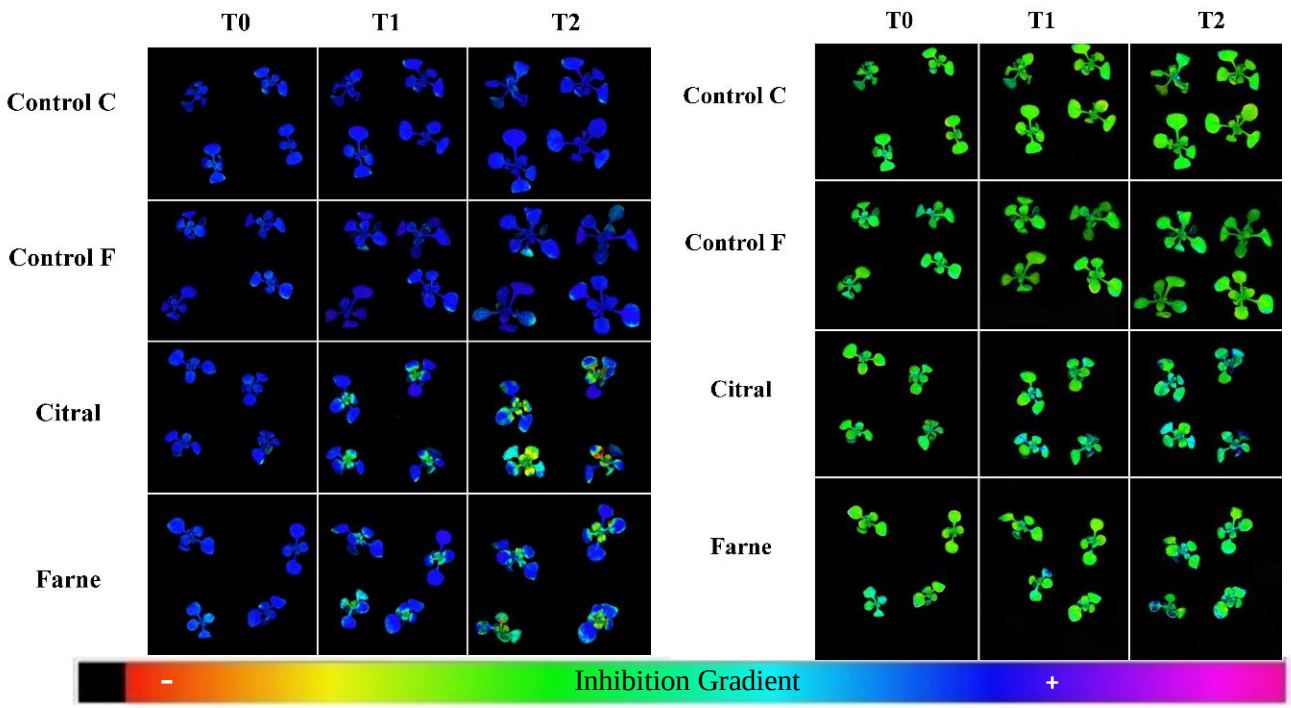

Figure 5. Pseudo-color images of dark-adapted PSII (*Fv/Fm*) (left) and of non-regulated energy emission as fluorescence (Φ_{NO}) (right) in *Arabidopsis* seedlings after farnesene and citral exposition. Images were taken at the beginning (T0) and at 24 (T1) and 48 h (T2) of treatment. Images of the different fluorescence parameters are depicted in false colors coding from 0.0 (black) to 1.0 (purple).

N= 4.

In parallel, a comparative study between farnesene and *cis*-citral isomer (also known as neral) was also done in *in silico* studies (farnesene *vs* citral) for DNA binding proteins on transcription factors previously found to be altered by citral (Graña et al., 2020). Table 3 shows that WHY-1, WHY-2, WHY-3, MYC-2 and NAC-1 were characterized by a very similar binding energy value for farnesene and citral, while different values were obtained when testing SHR_SCR.

Table 3. Binding energy scores between farnesene and citral on six different transcription factors (WHY-1, WHY-2, WHY-3, NAC, MYC and SHR-SCR) in ICM-docking studies. Nflex is the number of rotatable torsions; Eintl is internal conformation energy of the ligand; SolEl is the solvation electrostatics energy change upon binding; dTSc is the loss of entropy by the rotatable protein side-chains; Hbond is Hydrogen Bond energy.

PROTEIN	LIGAND	Score	Nflex	Eintl	SolEl	dTSsc	Hbond
WHY-1	Farnesene	-23.09	5	4.84	1.73	0.27	-
WHY-1	Neral	-23.40	3	1.93	5.65	0.81	-5.53
WHY-2	Farnesene	-20.33	5	1.16	1.51	1.04	-
WHY-2	Neral	-17.09	3	1.14	0.75	0.97	-1.92
WHY-3	Farnesene	-18.48	5	4.69	1.96	0.60	-
WHY-3	Neral	-20.85	3	2.63	1.92	0.56	-4.72
NAC-1	Farnesene	-18.48	5	3.60	6.86	1.11	-
NAC-1	Neral	-17.11	3	1.28	3.04	0.76	-2.23
MYC-2	Farnesene	-14.88	5	5.00	2.41	1.85	-
MYC-2	Neral	-19.26	3	3.68	3.15	0.94	-4.50
SHR_SCR	Farnesene	-15.70	5	4.60	3.42	1.48	-
SHR_SCR	Neral	-22.00	3	1.93	3.43	0.22	-4.44

As Graña et al. (2020) showed the interaction of the complex AtWHY-2-neral (cis isomer of citral) is the most effective, with spatial proximity between the ligand and two of the amino acids involved in binding to a specific ssDNA fragment (His 136 and Asp 137), which could effectively avoid the interaction between the amino acids WHY-2 and ssDNA, the *in silico* comparison of the effects of farnesene *vs* citral on this transcription factor was more deeply studied (Table 4). ICM Molecular modelling, carried out between AtWHY2 and farnesene or citral (Table 4), reported very similar results for both terpenoids. On

the contrary, as previously found with neral (Graña et al., 2020), farnesene is placed far from the union site with the DNA for AtWHY-1 and AtWHY-3, therefore not in-depth studies were done for these transcription factors in the present work.

Visual comparison of neral and farnesene reveals a high structural similarity, since the 1,5-octadienyl chain is present in both structures. Neral also possesses an aldehyde group that allows establishing hydrogen bonds with the side chains of the hydrophobic pocket residues, as shown in Table 4 (column N-HBond). However, the absence of a hydrogen bond acceptor oxygen atom in the polyene hydrocarbon structure of farnesene does not allow establishing this type of dipole-dipole interaction, which explains why the F-HBond values are all equal to 0. Table 4 also shows the interest of this comparison study between the two structures. Thus, in the farnesene structure, which presents a longer olefin, an increase in the contribution of the hydrophobic energy in the exposure of the ligand surface to water (F-Hphob column) and of the Vander waals interaction energies (F-VwInt column) is observed, maintaining good protein-ligand docking scores.

Table 4. ICM Molecular docking results of Farnesene (F) and Citral (N) on AtWHY2. Pose: protein-ligand binding sites; F-Score and N-Score = ICM scores; F-Hbond and N-Hbond = hydrogen bond energies; F-Hphob and N-Hphob = hydrophobic energies in exposing a surface to water; F-Vwint and N-Vwint = Vander waals interaction energies.

Pose	F-Score	N-Score	F-Hbond	N-Hbond	F-Hphob	N-Hphob	F-VwInt	N-VwInt
1	-20.33	-17.09	0.00	-1.92	-7.26	-4.94	-23.02	-16.58
2	-20.02	-16.67	0.00	-1.94	-7.31	-5.09	-22.95	-15.23
3	-19.08	-16.31	0.00	-1.82	-7.35	-4.50	-22.98	-17.36
4	-18.5	-15.84	0.00	-1.89	-7.32	-4.93	-21.89	-15.46
5	-18.49	-15.62	0.00	-1.86	-5.53	-4.68	-22.47	-15.96
6	-18.25	-15.13	0.00	-2.06	-7.08	-4.52	-23.03	-20.24
7	-18.2	-15.04	0.00	-1.36	-6.5	-4.93	-20.26	-16.95
8	-18.19	-14.72	0.00	-1.95	-7.21	-4.77	-22.85	-15.06

AtWHY2 is a whirly protein directed to mitochondria in *Arabidopsis* that has an assembled structure into a tetramer in solution (Cappadocia et al., 2013). This arrangement of protein chains results in a central hydrophobic pocket surrounded by residues, such as Phe198, Ala199, Pro201 or His202. The four lower-energy docked poses of farnesene on AtWHY2 in this binding site 1 (poses 1-4, table 4) could be

stabilized by hydrophobic interactions between its unsaturated alkyl chain and side groups of hydrophobic residues, which surround the central binding pocket, as can be seen in Fig. 6.

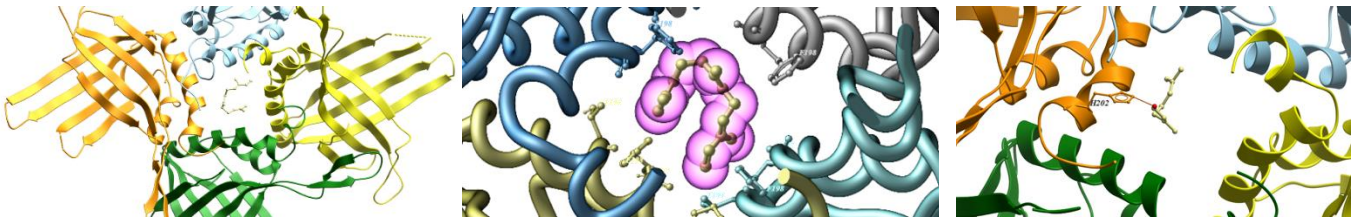

a b c

Figure 6. a) Farnesene structure (yellow) docked into the binding site of AtWHY-2 central hydrophobic pocket; b) volume area of farnesene and AtWHY2 residues less than 5A is shown; c) citral structure (yellow) docked into binding site 1 of AtWHY-2. Hydrogen bonds are shown as dotted orange lines.

At this same binding site 1, citral is also docked on AtWHY2 in an energetically favorable score (pose 5). The model further suggests the formation of a hydrogen bond between citral and a histidine residue (H_2O_2) that stabilizes the protein binding (Fig. 6b). However, the energetically more favorable binding pose 1 of citral is very similar to pose 5 (still energetically favorable) of farnesene at binding site 2 of the protein (Fig. 7a). In this binding site 2, farnesene shows a position slightly closer than citral to key residues for AtWHY2 (His136 and Asp 137), reported already in previous studies (Graña et al., 2020), suggesting a similar putative inhibition effect on WHY2-ssDNA binding (Fig. 7b).

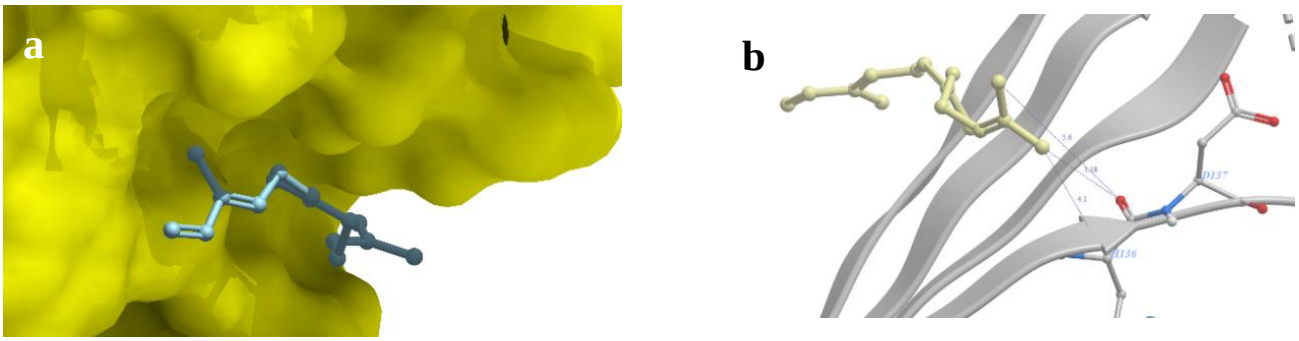

Figure 7. a) Pose 5 AtWHY2-Farnesene complex in binding site 2; b) proximity between farnesene (yellow) and two of the amino acids involved in binding to a specific ssDNA fragment (His 136 and Asp 137).

Regarding ANAC, other of the *in silico* studied binding proteins, it is interesting to highlight that the structure of the NAC domain is arranged as a dimer in solution (Ernst et al., 2004). Two saline bridges

formed by conserved Arg19 and Glu26 stand out among the residues involved in the union between dimers. In addition, an antiparallel beta-sheet is formed, cutting the dimer interface, with hydrogen bonds between Arg19…Arg19 and Tyr21…Gly17. In ICM molecular docking studies, all poses that energetically favor the binding of citral and farnesene metabolites on ANAC showed an arrangement of ligands at the binding site between NAC monomers. Citral has a hydrogen bond with a Gly17 residue (Fig. 8a), which stabilizes this pose; while farnesene is close to the antiparallel beta-sheet, specifically to Arg19 residue (Fig. 8b). Both ligands could make it challenging to stabilize the NAC dimer for ssDNA binding.

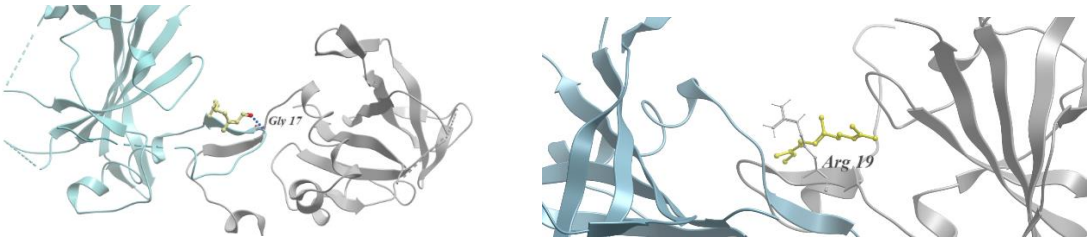

a) b)

Figure 8. a) Citral structure (yellow) docked into the binding site of NAC. Hydrogen bonds are shown as dotted green lines; b) Farnesene structure (yellow) docked into the binding site of NAC.

The comparative study of the effect on DNA binding proteins of farnesene *vs* neral (citral isomer) on SHR-SCR complex was also done. In this case, the comparative study between the ICM docking results of farnesene and citral against the SHR-SCR complex showed a different behaviour of both terpenes, as SHR-SCR-farnesene ICM docking results predicted a less favourable protein-ligand binding energy (Table 3). Furthermore, the interaction sites were very different in all poses. Similar results were obtained in the comparative study for the interaction of farnesene and neral with MYC-2, as neral showed better ICM docking than farnesene with score values of -19.26 and -14.88, respectively, and a hydrogen bound with the Lys 480 and Ser 479 residues (Fig. 9).

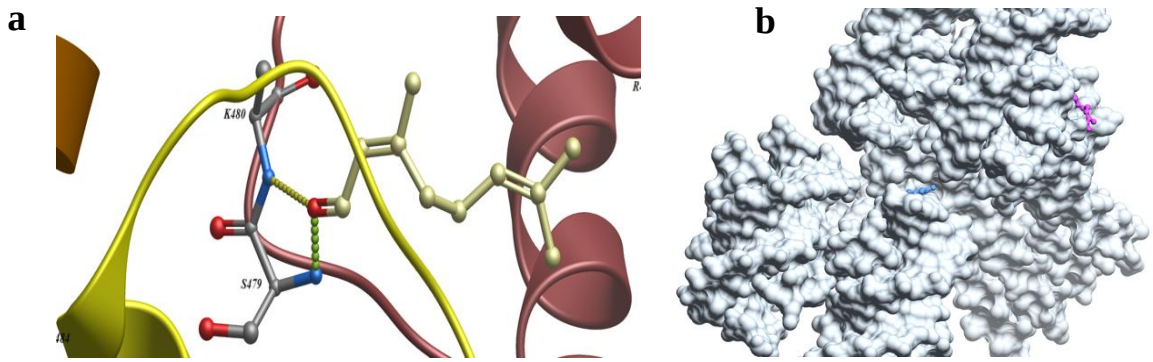

Figure 9. a) ICM-Pro docking model of neral (yellow) binding to MYC: hydrogen bonds are coloured as green and yellow dotted lines; b) ICM-Pro docking model binding of neral and farnesene to MYC in a toggle skin representation. Farnesene is coloured as pink and neral as blue.

DISCUSSION

The comparative metabolomics study revealed significant similarities but also differences between the two molecules. It is important to remember that the measuring times used in this work for comparing citral and farnesene effects were set up at 24 and 48 h to allow protein codification, enzymatic reactions and metabolites' synthesis as a a consequence of the effects observed with citral. If there are any errors during gene transcription, this could affect protein synthesis and enzyme activity in both roots and leaves. Regardless of the organ affected, these alterations could have consequences on functions performed by the plant, such as photosynthesis.

Both PCA and PLS-DA analyses, carried out on the annotated metabolites, highlighted a clear separation of the two molecules, which resided on two different quadrants. Also, the pathways analysis highlighted that both molecules were affecting similar pathways but to a different extent, as previously found for the fluorescence measurements.

The univariate analysis evidenced a clear similitude in the changes in concentration of specific compound classes. In particular, both terpenoids caused a decrease in most of the sugars, mainly glucose and sucrose, whose levels were significantly altered. The reduction of these sugars has been observed in *Arabidopsis* cells subjected to oxidative stress (Baxter et al., 2007) and in *Arabidopsis* roots isolated from seedlings treated with the natural compound rosmarinic acid (Araniti et al., 2018a). Low levels of sugars, especially the reduction in sucrose content caused by both compounds, might be due to the observed reduction in photosynthetic efficiency. Araniti et al. (2018b) observed that using *Origanum vulgare*

essential oils, whose composition is mainly based on the mixture of many terpenes, caused a reduction in photosynthetic efficiency and sucrose content, as observed in our assay. Sugar reduction could also have a side effect on the TCA cycle, one of the pathways affected by both compounds. Moreover, a reduction in pyruvate was observed in treated plants, which is known to be pivotal for the TCA cycle efficiency (Fernie et al, 2004).

The general decrease in sucrose content found in metabolomic analyses for both terpenoids after 24 and 48 h was the reason for performing chlorophyll *a* fluorescence, since it represents the main photosynthetic product.

The analysis carried out on treated seedlings showed that the PSII apparatus of *Arabidopsis* seedlings were similarly affected by both compounds and these effects were more significant after 48 h of treatment. The results indicated that the photosynthetic efficiency of PSII severely decreased for both compounds in treated seedlings, while a parallel increase of Φ_{NPQ} and Φ_{NO} was observed.

Φ_{NPQ} represents the fraction of energy dissipated via the regulated photoprotective NPQ (non-photochemical quenching) mechanisms in the form of heat [Δ-pH- and xanthophyll-regulated thermal dissipation; (Sánchez-Moreiras et al., 2020)]. The observed increment of this parameter after treatment with citral and farnesene suggests that excessive excitation energy can be efficiently dissipated into harmless heat and the PSII energy regulation mechanism. However, farnesene-treated plants maintained the the ability to dissipate the neregy in excess in the form of heat all over the treatment more than citral. In fact, the decrease of Φ_{NPQ} in 48 h citral-treated plants suggested that the plants cannot anymore compensate the excess of energy through a controlled energy emission Moreover, when plants were exposed to saturating light intensities, an increase of Φ_{NO} over Φ_{NPQ} reflected a suboptimal capacity of photoprotective reactions, eventually leading to photodamage and successively to chronic photoinhibition (Klughammer and Schreiber, 2008), as Φ_{NO} reflects the fraction of energy emitted mainly in the form of fluorescence as a consequence of closed PSII (Klughammer and Schreiber, 2008; Pfündel et al., 2008). For example, the previously described ability of these molecules to induce oxidative stress in *Arabidopsis* (Araniti et al., 2016; Graña et al., 2013) could be speculated to be a direct consequence of a reduced ability in processing light, probably due to an increase of close or damaged reaction centers, which leads to further ROS generation and propagation of oxidative stress, even at the level of chloroplast membrane.

Such ROS-guided phenomena are generally accompanied by a reduction of the dark-adapted PSII efficiency (F_v/F_m), significantly affected in our experiments, which indicates that the physiological status of the plant was altered, and a situation of photoinhibition or reduction of PSII activity is occurring

(Bresson et al., 2015). Looking at the images of F_v/F_m it is possible to observe that the citral- and farnesene-induced damages begin at the center of the rosette after 24 h of treatment and then extend to the rest of the shoot. This decrease may be a sign of physical damage to the PSII, as Graña et al. (2013a) observed. To protect the antenna complex in these situations, plants can dissipate excess energy through the previously described Φ_{NPQ} mechanism, which was strongly stimulated in our experiments, suggesting that plants treated can face stress in the short period. However, if the treatment time is prolonged, the harmful fluorescence energy emission (Φ_{NO}) is the predominant way of energy dissipation. This trend was highlighted and confirmed in the false color scale image of Φ_{NO} parameter, where a time-dependent stress progression can be observed. In addition, the alteration of the previously described parameters was accompanied by a reduction of the light-adapted PSII efficiency (Φ_{II}), confirming that plants were in a stress situation, and the energy dissipation mechanisms started to fail, especially faster in citral than in farnesene-treated plants (Kramer et al., 2004). These results are similar to the effects of the indole alkaloid norharmane assayed on adult plants of *A. thaliana* (López-González et al., 2020). Finally, the observed decrease in ETR might indicate failures in the biochemical phase of photosynthesis, such that electrons cannot reach their final acceptors (Oikonomou et al., 2019).

However, the pathways most affected by the treatments were related to amino acid metabolism, which significantly accumulated after molecules treatment to a different extent (more in citral-treated seedlings than in farnesene). Increases in amino acids such as GABA, proline or asparagine are related to stress resistance processes (Szabados and Savouré, 2009). In particular, proline can accumulate under oxidative stress to protect membranes and act as a scavenger of reactive species (Kishor and Sreenivasulu, 2014), while GABA levels increase under biotic and abiotic stress (Bouché and Fromm 2004). Another amino acid accumulated after treatments with a pivotal role in regulating cellular redox homeostasis under stress is glutamine (Ji et al., 2019), This accumulation of glutamine may be related to the observed urea reduction. The enzyme urease degrades urea to NH_3, which would be transformed with glutamate into glutamine by the action of the enzyme glutamine synthetase (GS) (Witte 2019). The observed increase in polyamines is also related to plant stress response (Podlešáková et al., 2019), and the increase in lysine and threonine levels is related to the synthesis of stress-specific proteins, as they are their typical components (Waters et al., 1996).

Moreover, the amino acid metabolic profiles obtained after citral and farnesene treatments were very similar to that observed on *Arabidopsis* plants treated with the terpenoid-alcohol nerolidol (Landi et al., 2020) and on lettuce plants exposed to the volatiles produced by the potentially allelopathic species *Dittrichia viscosa* (Araniti et al., 2017b). These results suggest that plants are experiencing oxidative

stress and are modulating their metabolism to face it, increasing the production of osmoprotectants (polyamine and quaternary ammonium compounds) and activating the previously described photoprotective mechanisms (Φ_{NPQ} and Φ_{NO}). In addition, a high accumulation of serine in plants was observed, which is an amino acid of great importance during the photorespiratory cycle (Bourguignon et al.,1998). Photorespiration is a process that, in stressful situations, can serve as an electron sink to maintain a correct flow of electrons and thus prevent oxidative damage (Osei-Bunsu et al., 2020). A negative correlation between photorespiration and ETR, as well as a positive correlation with proline content, has been observed under stress (Ünlüsoy et al., 2022). Thus, photorespiration would be activated after citral and farnesene treatment to compensate for the loss of photosynthetic capacity and prevent oxidative damage. However, the faster occurrence of metabolites content alterations in citral when compared to farnesene suggests that citral could be acting faster than farnesene in the *Arabidopsis* metabolism, which could also explain the stronger effect of citral on fluorescence parameters and the higher amounts of metabolites affected by citral in 24 h, which are reached by farnesene after 48 h of treatment.

The quicker toxic effect exerted by citral in comparison with farnesene can also be confirmed by observing the differential effects highlighted by the pathway analysis.

The comparison of 24 h citral treatment with 24 h farnesene treatment highlighted that among the 11 metabolic pathways with the highest impact, 5 routes were significantly affected by farnesene. In contrast, 8 routes were significantly affected by citral, demonstrating the ability of citral to alter the metabolism of early-treated seedlings quicker than farnesene. The routes altered by citral but not by farnesene were alanine aspartate and glutamate metabolism, citrate cycle (TCA cycle) and tryptophan metabolism.

For example, compounds belonging to the TCA cycle such as fumaric acid, pyruvic and citric acid significantly dropped down in citral treatment after 24 h. On the contrary, only fumaric and pyruvic acid in farnesene treatments were significantly inhibited after 48 h of treatment.

This alteration in the TCA cycle can affect the synthesis of amino acids such as aspartic acid (Lehmann et al., 2012; Savchenko and Tikhonov, 2021), thus altering the alanine, aspartate and glutamate metabolism, evidenced by the reduction in aspartate levels in 24 h citral treatment. This pathway is also affected by increased alanine levels, often elevated in stressful situations (Monselise, 2011). Miyashita and Good (2008) observed an accumulation of alanine in *A. thaliana* roots under hypoxia. Concerning tryptophan metabolism, Graña et al. (2013a) found that *A. thaliana* seedlings showed an increase in auxin content after 5 and 10 h of citral treatment, a phytohormone that can be biosynthesized in plants from

tryptophan (Morffy and Strader, 2020). After 48 h, the number of significantly altered pathways increases in both treatments. Considering the 11 altered pathways significantly impacted by the treatments, in the case of farnesene, there were 9 altered pathways while treatment with citral affected 10 pathways, with both treatments just differing in the tryptophan pathway, which was affected by citral but not by farnesene. This suggests a very similar behaviour in the mode of action of farnesene and citral in the treated seedlings. Whereas citral has been proven to alter the auxin balance in *Arabidopsis* seedlings (Graña et al., 2013), Araniti et al. (2017a) also demonstrated that farnesene-induced root growth alterations were mainly due to an altered distribution of auxin due to the inhibition of PIN proteins involved in auxin redistribution.

Focusing more on the effects, also the *in-silico* analysis highlighted similarities and differences between citral and farnesene. Graña et al. (2020) recently showed, through transcriptomic and *in silico* studies, that the mechanism of phytotoxicity of citral involves the interaction of citral isomers with single strand DNA binding proteins (SSBPs) inducing an almost total blockage of the plant metabolism in the first hours of citral treatment. Therefore, *in silico* molecular docking analysis was done in our study to compare citral and farnesene capacity to interact with SSBPs. *In silico* studies suggested binding of citral isomers and farnesene to the single strand DNA binding protein WHY2 and to other transcription factors such as ANAC, while not interesting interactions were observed for both compounds with WHY-1 and WHY-3. In fact, there is a clear similarity in the interaction of farnesene and citral with SSBPs, although also some differences were found in the mechanism of action of these two compounds. In particular, the main differences were related to the protein scarecrow (SCR) and MYC-2, located in root tissues, which were characterized by a higher affinity for citral (neral) than for farnesene, which could be related to the quicker action of citral in comparison with farnesene. For neral (citral), two hydrogen bonds with residues G584 and S583 were observed in the SHR-SCR-citral ICM docking and with L480 and S479 in the MYC-2-citral ICM docking in an energetically stabilized pose by the formation of a five-membered cycle, as indicated in a previous article (Graña et al., 2020), suggesting that these interactions could alter the binding of SCR-SHR and MYC-2 to ssDNA. However, these key interactions could not be observed in ICM docking studies between SHR-SCR and MYC-2 with farnesene. The ICM molecular docking models suggests that ligands binding sites for SCR and MYC-2 are located in different positions for neral and farnesene. While neral is located in a buried hydrophobic pocket, farnesene is located on the surface, in a water-exposed position. The low affinity of farnesene to SCR agrees with Araniti et al. (2017a), which demonstrated that *Arabidopsis* root treatment with this molecule (at the ED50 concentration) strongly affected PIN proteins but did not affect SCR distribution. The fast ability of the monoterpenoid

citral (C10, a much smaller molecule than farnesene) to enter in the DNA helix and interact with key positions of the DNA transcription can be the reason for the faster effect of citral on *Arabidopsis* (with an almost complete blockage of gene expression in the first minutes of treatment; Graña et al., 2020), when compared to the sesquiterpene farnesene (C15). Previous genotoxic studies have shown that disrupted DNA replication and transcription can affect genome stability, resulting in reduced protein synthesis, damage of cell membrane and photosynthetic proteins (Dutta et al., 2018), oxidative stress, and finally plant growth and development alterations, as shown for farnesene and citral.

Conclusions

Both metabolomic analysis and *in-silico* studies highlighted clear similarities in the metabolic pathways and metabolites profile affected by these two chemicals at different times but also differences concerning the affinity with the proteins with which they could potentially interact, suggesting a faster effect of citral when compared to farnesene but also the ability of citral to affect pathways (i.e. tryptophan route) not affected by farnesene. Those results suggest that the two molecules share many of the mechanisms of action on plant metabolism, especially those related to the immediate interaction with DNA binding proteins and the induction of oxidative stress, while the damage to the photosynthetic machinery could be a side effect due to a potential increase in ROS after both molecules' treatment. The apparent harmlessness of these compounds to other organisms together with their effect on plant metabolism make these compounds excellent candidates for further study of their mode of action in search of new natural molecules with potential herbicidal activity.

Acknowledgement

The MS was funded by the "Ministerio de Ciencia, Innovaciòn y Universidades" [grant code RTI2018-094716-B-100].

Data availability statement

The datasets generated during and/or analysed during the current study are available from the corresponding author on reasonable request.

Bibliography

Abagyan, R., Totrov, M., 1994. Biased probability Monte Carlo conformational searches and electrostatic calculations for peptides and proteins. J Mol Biol 235, 983–1002. https://doi.org/10.1006/jmbi.1994.1052.

Abagyan, R., Totrov, M., Kuznetsov, D., 1994. ICM-A New method for protein modeling and design: Applications to docking and structure prediction from the distorted native vonformation. J Comput Chem 15, 488–506. https://doi.org/https://doi.org/10.1002/jcc.540150503.

Aliferis, K.A., 2020. Metabolomics in plant protection product research and development: discovering the mode(s)-of-action and mechanisms of toxicity, in: Álvarez-Muñoz, D., Farré, M. (Eds.), Environmental Metabolomics Applications in Field and Laboratory Studies to Understand from Exposome to Metabolome. Elsevier, pp. 163–194.

Araniti, F., Costas-Gil, A., Cabeiras-Freijanes, L., Lupini, A., Sunseri, F., Reigosa, M. J., Abenavoli, M.R., Sanchez-Moreiras, A. M., 2018a. Rosmarinic acid induces programmed cell death in *Arabidopsis* seedlings through reactive oxygen species and mitochondrial dysfunction. PloS One, 13, e0208802. https://doi.org/10.1371/journal.pone.0208802.

Araniti, F., Bruno, L., Sunseri, F., Pacenza, M., Forgione, I., Bitonti, M.B., Abenavoli, M.R., 2017a. The allelochemical farnesene affects *Arabidopsis thaliana* root meristem altering auxin distribution. Plant Physiol. Biochem. 121, 14–20. https://doi.org/10.1016/j.plaphy.2017.10.005.

Araniti, F., Graña, E., Krasuska, U., Bogatek, R., Reigosa, M.J., Abenavoli, M.R., Sánchez-Moreiras, A.M., 2016. Loss of gravitropism in farnesene-treated arabidopsis is due to microtubule malformations related to hormonal and ROS unbalance. PLoS One 11, e0160202 . https://doi.org/10.1371/journal.pone.0160202.

Araniti, F., Graña, E., Reigosa, M.J., Sánchez-Moreiras, A.M., Abenavoli, M.R., 2013. Individual and joint activity of terpenoids, isolated from *Calamintha nepeta* extract, on *Arabidopsis thaliana*. Nat Prod Res 27, 2297–2303. https://doi.org/10.1080/14786419.2013.827193.

Araniti, F., Landi, M., Lupini, A., Sunseri, F., Guidi, L., Abenavoli, M. R., 2018b. *Origanum vulgare* essential oils inhibit glutamate and aspartate metabolism altering the photorespiratory pathway in *Arabidopsis thaliana* seedlings. J. Plant Physiol 231, 297–309. https://doi.org/10.1016/j.jplph.2018.10.006.

Araniti, F., Lupini, A., Sunseri, F., Abenavoli, M.R., 2017b. Allelopatic potential of *Dittrichia viscosa* (L.) W. Greuter mediated by VOCs: A physiological and metabolomic approach. PLoS One 12, e0170161. https://doi.org/10.1371/journal.pone.0170161.

Araniti, F., Miras-Moreno, B., Lucini, L., Landi, M., Abenavoli, M.R., 2020. Metabolomic, proteomic and physiological insights into the potential mode of action of thymol, a phytotoxic natural monoterpenoid phenol. Plant Physiology and Biochemistry 153, 141–153. https://doi.org/10.1016/j.plaphy.2020.05.008.

Baxter, C.J., Redestig, H., Schauer, N., Repsilber, D., Patil, K.R., Nielsen, J., Selbig, J., Liu, J., Fernie, A.R., Sweetlove, L.J., 2007. The metabolic response of heterotrophic *Arabidopsis* cells to oxidative stress. Plant Physiol 143, 312–325. https://doi.org/10.1104/pp.106.090431.

Bouché, N., Fromm, H., 2004. GABA in plants: Just a metabolite? Trends Plant Sci 9, 110–115. https://doi.org/10.1016/j.tplants.2004.01.006.

Bourguignon, J., Ribeilli, F., Douce, R., 1999. Serine and glycine metabolism in higher plants, in: Singh, B.K. (Ed.), Plant amino acids Biochemistry and Biotechnology. CRC Press, Boca Raton, pp. 111–146. https://doi.org/https://doi.org/10.1201/9781482270068.

Bresson, J., Vasseur, F., Dauzat, M., Koch, G., Granier, C., Vile, D., 2015. Quantifying spatial heterogeneity of chlorophyll fluorescence during plant growth and in response to water stress. Plant Methods 11, 1–15. https://doi.org/10.1186/s13007-015-0067-5.

Cappadocia, L., Parent, J.S., Sygusch, J., Brisson, N., 2013. A family portrait: Structural comparison of the Whirly proteins from *Arabidopsis thaliana* and *Solanum tuberosum*. Acta Crystallograph 69, 1207–1211. https://doi.org/10.1107/S1744309113028698.

Çelik, K., Toğar, B., Türkez, H., Taşpinar, N., 2014. In vitro cytotoxic, genotoxic, and oxidative effects of acyclic sesquiterpene farnesene. Turk J Biol 38, 253–259. https://doi.org/10.3906/biy-1309-55.

Chaimovitsh, D., Rogovoy Stelmakh, O., Altshuler, O., Belausov, E., Abu-Abied, M., Rubin, B., Sadot, E., Dudai, N., 2012. The relative effect of citral on mitotic microtubules in wheat roots and BY2 cells. Plant Biol 14, 354–364. https://doi.org/10.1111/j.1438-8677.2011.00511.x.

Duke, S., Pan, Z., Bajsa-Hirshel, J., Sánchez-Moreiras, A.M., Vaughn, J., 2018 Use of omics methods to determine the mode of action of natural phytotoxins, in: Beck, J. J., Rering, C. C., Duke, S. O., (Eds), Roles of Natural Products for Biorational Pesticides in Agriculture. ACS Symposium Series, pp. 33–46. doi: 10.1021/bk-2018-1294.ch005.

Duke, S.O., Dayan, F.E., 2022. The search for new herbicide mechanisms of action: Is there a 'holy grail'? Pest Manag Sci 78, 1303–1313. https://doi.org/10.1002/ps.6726.

Duke, S.O., Stidham, M.A., Dayan, F.E., 2019. A novel genomic approach to herbicide and herbicide mode of action discovery. Pest Manag Sci 75, 314–317. https://doi.org/10.1002/ps.5228.

Dutta S, Mitra M, Agarwal P, Mahapatra K, De S, Sett U, Roy S. 2018. Oxidative and genotoxic damages in plants in response to heavy metal stress and maintenance of genome stability. Plant Signal Behav 13, e1460048. doi: 10.1080/15592324.2018.1460048.

Fagodia, S.K., Singh, H.P., Batish, D.R., Kohli, R.K., 2017. Phytotoxicity and cytotoxicity of *Citrus aurantiifolia* essential oil and its major constituents: Limonene and citral. Ind Crops Prod 108, 708–715. https://doi.org/10.1016/j.indcrop.2017.07.005.

Fernie, A.R., Carrari, F., Sweetlove, L.J., 2004. Respiratory metabolism: Glycolysis, the TCA cycle and mitochondrial electron transport. Curr Opin Plant Biol 7, 254–261. https://doi.org/10.1016/j.pbi.2004.03.007.

Gaines, T. A., Duke, S. O., Morran, S., Rigon, C. A., Tranel, P. J., Küpper, A., Dayan, F. E., 2020. Mechanisms of evolved herbicide resistance. J. Biol. Chem., 295, 10307–10330. https://doi.org/10.1074/jbc.REV120.013572.

Graña, E., Díaz-Tielas, C., Sánchez-Moreiras, A.M., Reigosa, M.J., Celeiro, M., Abagyan, R., Teijeira, M., Duke, M. v., Clerk, T., Pan, Z., Duke, S.O., 2020. Transcriptome and binding data indicate that citral inhibits single strand DNA-binding proteins. Physiol Plant 169, 99–109. https://doi.org/10.1111/ppl.13055.

Graña, E., Sotelo, T., Díaz-Tielas, C., Araniti, F., Krasuska, U., Bogatek, R., Reigosa, M.J., Sánchez-Moreiras, A.M., 2013a. Citral induces auxin and ethylene-mediated malformations and arrests cell division in *Arabidopsis thaliana* roots. J Chem Ecol 39, 271–282. https://doi.org/10.1007/s10886-013-0250-y.

Graña, Elisa, Sotelo, T., Díaz-Tielas, C., Reigosa, M.J., Sánchez-Moreiras, A.M., 2013b. The phytotoxic potential of the terpenoid citral on seedlings and adult plants. Weed Sci 61, 469–481. https://doi.org/10.1614/ws-d-12-00159.1.

Gressel, J., 2020. Perspective: present pesticide discovery paradigms promote the evolution of resistance–learn from nature and prioritize multi- target site inhibitor design. Pest Manag. Sci., 76, 421–425. https://doi.org/10.1002/ps.5649.

Hachisu, S., 2021. Strategies for discovering resistance-breaking, safe and sustainable commercial herbicides with novel modes of action and chemotypes. Pest Manag Sci 77, 3042–3048. https://doi.org/10.1002/ps.6397.

Ji, Y., Li, Q., Liu, G., Selvaraj, G., Zheng, Z., Zou, J., Wei, Y., 2019. Roles of cytosolic glutamine synthetases in *Arabidopsis* development and stress responses. Plant Cell Physiol 60, 657–671. https://doi.org/10.1093/pcp/pcy235.

Kavi Kishor, P.B., Sreenivasulu, N., 2014. Is proline accumulation per se correlated with stress tolerance or is proline homeostasis a more critical issue? Plant Cell Environ 37, 300–311. https://doi.org/10.1111/pce.12157.

Klughammer, C., Schreiber, U., 2008. Complementary PS II quantum yields calculated from simple fluorescence parameters measured by PAM fluorometry and the Saturation Pulse method. PAM Application Notes 1, 27–35.

Kramer, D.M., Johnson, G., Kiirats, O., Edwards, G.E., 2004. New fluorescence parameters for the determination of Q A redox state and excitation energy fluxes. Photosynth Res 79, 209–218. https://doi.org/https://doi.org/10.1023/B:PRES.0000015391.99477.0d.

Landi, M., Misra, B.B., Muto, A., Bruno, L., Araniti, F., 2020. Phytotoxicity, morphological, and metabolic effects of the sesquiterpenoid nerolidol on *Arabidopsis thaliana* seedling roots. Plants 9, 1–19. https://doi.org/10.3390/plants9101347.

López- González, D., Ledo, D., Cabeiras- Freijanes, L., Verdeguer, M., Reigosa, M.J., Sánchez- Moreiras, A.M., 2020. Phytotoxic activity of the natural compound norharmane on crops, weeds and model plants. Plants 9, 1–23. https://doi.org/10.3390/plants9101328.

Martínez-Peñalver, A., Reigosa, M.J., Sánchez-Moreiras, A.M., 2011. Imaging chlorophyll *a* fluorescence reveals specific spatial distributions under different stress conditions. Flora: Morphology, Distribution, Functional Ecology of Plants 206, 836–844. https://doi.org/10.1016/j.flora.2011.02.004.

Oikonomou, A., Ladikou, E.V., Chatziperou, G., Margaritopoulou, T., Landi, M., Sotiropoulos, T., Araniti, F., Papadakis, I.E., 2019. Boron excess imbalances root/shoot allometry, photosynthetic and chlorophyll fluorescence parameters and sugar metabolism in apple plants. Agronomy 9, 1–17. https://doi.org/10.3390/agronomy9110731.

Osei- Bonsu, I., McClain, A. M., Walker, B. J., Sharkey, T. D., Kramer, D. M., 2021. The roles of photorespiration and alternative electron acceptors in the responses of photosynthesis to elevated temperatures in cowpea. Plant Cell Environ., 44, 2290–2307. https://doi.org/10.1111/pce.14026.

Podlešáková, K., Ugena, L., Spíchal, L., Doležal, K., de Diego, N., 2019. Phytohormones and polyamines regulate plant stress responses by altering GABA pathway. N Biotechnol 48, 53–65. https://doi.org/10.1016/j.nbt.2018.07.003.

Sánchez-Moreiras, A.M., Graña, E., Reigosa, M.J., Araniti, F., 2020. Imaging of chlorophyll *a* fluorescence in natural compound-induced stress detection. Front Plant Sci 11, 583590. https://doi.org/10.3389/fpls.2020.583590.

Schapira M, Totrov M, Abagyan R (1999) Prediction of the binding energy for small molecules, peptides and proteins J Mol Recognit 12, 177–190. https://doi.org/10.1002/(SICI)1099-1352(199905/06)12:3<177::AID-JMR451>3.0.CO;2-Z.

Szabados, L., Savouré, A., 2010. Proline: a multifunctional amino acid. Trends Plant Sci 15, 89–97. https://doi.org/10.1016/j.tplants.2009.11.009.

Trenkamp, S., Eckes, P., Busch, M., Fernie, A.R., 2009. Temporally resolved GC-MS-based metabolic profiling of herbicide treated plants treated reveals that changes in polar primary metabolites alone can distinguish herbicides of differing mode of action. Metabolomics 5, 277–291. https://doi.org/10.1007/s11306-008-0149-8.

Ünlüsoy, A. G., Yolcu, S., Bor, M., Özdemir, F., Türkan, İ., 2022. Activation of photorespiration facilitates drought stress tolerance in *Lotus corniculatus*. J. Plant Growth Regul., 1–14. https://doi.org/10.1007/s00344-022-10683-5.

Vaughn, S.F., Spencer, G.F., 1993. Volatile monoterpenes as potential parent structures for new herbicides. Weed Sci 41, 114–119. https://doi.org/10.1017/S0043174500057672.

Verdeguer, M., Sánchez-Moreiras, A.M., Araniti, F., 2020. Phytotoxic effects and mechanism of action of essential oils and terpenoids. Plants 9, 1–52. https://doi.org/10.3390/plants9111571.

Vuorinen, T., Reddy, G.V.P., Nerg, A.M., Holopainen, J.K., 2004. Monoterpene and herbivore-induced emissions from cabbage plants grown at elevated atmospheric CO_2 concentration. Atmos Environ 38, 675–682. https://doi.org/10.1016/j.atmosenv.2003.10.029.

Waters, E.R., Lee, G.J., Vierling, E., 1996. Evolution, structure and function of the small heat shock proteins in plants. J Exp Bot 47, 325–338. https://doi.org/https://doi.org/10.1093/jxb/47.3.325.

Witte, C. P., 2011. Urea metabolism in plants. Plant Sci, 180, 431–438. https://doi.org/10.1016/j.plantsci.2010.11.01.

Xia, J., Sinelnikov, I. v., Han, B., Wishart, D.S., 2015. MetaboAnalyst 3.0-making metabolomics more meaningful. Nucleic Acids Res 43, W251–W257. https://doi.org/10.1093/nar/gkv380.

Similarities on the mode of action of the terpenoids citral and farnesene in *Arabidopsis* seedlings involve interactions with DNA binding proteins

López-González D[1], Graña E[1], Teijeira M[2,3], Verdeguer M[4], Reigosa MJ[1], Sánchez-Moreiras AM[1*], Araniti F[5*]

[1]Universidade de Vigo. Departamento de Bioloxía Vexetal e Ciencia do Solo, Facultade de Bioloxía. Campus Lagoas-Marcosende s/n, 36310 Vigo, Spain;

[2] Universidade de Vigo, Departamento de Química Orgánica, Facultade de Química, 36310 Vigo, Spain; qomaca@uvigo.es

[3] Instituto de Investigación Sanitaria Galicia Sur, Hospital Álvaro Cunqueiro, 36213 Vigo, Spain

[4]Instituto Agroforestal Mediterráneo (IAM), Universitat Politècnica de València, Camino de Vera s/n, 46022 Valencia, Spain

[5]Dipartamento di Science Agrarie e Ambientali – Produzione, Territorio, Agroenergia, Università Statale di Milano, Via Celoria n º2, 20133 Milano, Italy

Corresponding Authors:

F. Araniti fabrizio.araniti@unimi.it,

A.M. Sánchez-Moreiras adela@uvigo.es

Field Code Changed

Field Code Changed

Abstract

The sesquiterpene farnesene and the monoterpene citral are phytotoxic natural compounds characterized by a high similarity in macroscopic effects, suggesting an equal or similar mechanism of action when assayed at IC_{50} concentration. In the present study, a short-time experiment (24 and 48 h) using an imaging spectrofluorometer allowed us to monitor the *in-vivo* effects of the two molecules, highlighting that both terpenoids were similarly affecting all PSII parameters, even when the effects of citral were quicker in appearing than those of farnesene. The multivariate, univariate, and pathway analyses, carried out on untargeted-metabolomic data, confirmed a clear separation of the plant metabolome in response to the two treatments, whereas similarity in the affected pathways was observed. The main metabolites affected were amino acids and polyamine, which significantly accumulated in response to both treatments. On the contrary, a reduction in sugar content (i.e. glucose and sucrose) was observed. Finally, the *in-silico* studies demonstrated a similar mechanism of action for both molecules by interacting with DNA binding proteins, although differences concerning the affinity with the proteins with which they could potentially interact were also highlighted. Despite the similarities in macroscopic effects of these two molecules, the metabolomic and *in-silico* data suggest that both terpenoids share a similar but not equal mechanism of action and that the similar effects observed on the photosynthetic machinery are more imputable to a side effect of molecules-induced oxidative stress.

Keywords: *Arabidopsis thaliana*, chlorophyll *a* fluorescence, *in silico* studies, metabolomics, molecular docking, natural compounds.

INTRODUCTION

Weeds are one of the main problems farmers face, as they compete with crops for edaphic resources, causing a loss in crop yield and quality (Hachisu, 2021). The quickest and cheapest solution for many farmers is the use of synthetic herbicides, a common practice for the last 70 years (Duke et al., 2018). However, these compounds have numerous adverse effects, such as being harmful to the environment or human health, and the emergence of resistant weeds due to their indiscriminate use. Only one herbicide with a new MOA (cyclopyrimorate) has been introduced on the market since 1980, and one is close to being introduced (tetflupyrolimet) (Duke and Dayan, 2021), but no more herbicides with new modes of action (MOAs) have been discovered in the last 30-40 years. This is why searching for new molecules with a potential bioherbicidal capacity that presents new molecular targets is necessary.

Natural compounds are a source of new pesticides with potential new modes of action, different from those of current herbicides, which could help to tackle the problem of weed's resistance (Duke et al., 2018). In addition, it is possible that a natural compound with an already known MOA is effective against a weed with resistance to that MOA, as the structural diversity of natural compounds allows them to bind to the target site differently from the conventional herbicide and become effective (Duke and Dayan 2021). Moreover, many natural compounds have been found to show more than one molecular target site and more than one MOA, which makes them more effective in avoiding weed resistance (Duke et al., 2020; Gressel 2020). For example, the natural compound sorgoleone inhibits the D2 protein in the photosystem II (PSII) and also inhibits the enzyme 4-hydroxyphenylpyruvate dioxygenase (involved in PSII plastoquinone synthesis), and linarin inhibits seed respiration, germination, root and hair growth and the donor side of PSII (Gressel 2020).

Recently, the use of *-omics* techniques and molecular, biochemical and physiological techniques has significantly impacted the study of the effect of natural compounds on plant metabolism (Araniti et al., 2020). Of all the omics, metabolomics is the one that explains the phenotype by correlating it with changes in the metabolome. Studying the metabolome and its changes in response to bioactive compounds can generate important information on the MOA of natural compounds (Aliferis, 2020). For example, Trenkamp et al. (2009) used GC-MS to observe the effects of various herbicides (glufosinate, glyphosate, sulcotrione, etc.) on the metabolome of *A. thaliana*. Moreover, recently, metabolomics has begun to be widely used in studying the stresses and mechanisms of action of natural molecules with potential bioherbicide activity (Shualev et al, 2008; Misra et al., 2020).

Among these specialized metabolites with potential bioherbicide activities, terpenoids are one of the classes characterized by a significant biological activity widely studied in the last years (Verdeguer et al., 2020).

The monoterpene citral, firstly characterized in the essential oil of *Citrus aurantiifolia*, is an interesting terpenoid with strongly demonstrated phytotoxicity (Chaimovitsh et al., 2012; Graña et al., 2013b). Vaughn and Spencer (1993) were the first to show that the saturation of desiccator flasks with citral vapours induced a 32, 80 and 96% inhibition of germination of maize, soybean and cucumber, respectively. When used in solution, it was phytotoxic for lettuce, barley, wild oat, ribwort, redroot pigweed and barnyard grass and caused oxidative damage to *A. thaliana* (Graña et al., 2013a). This compound also induced the disorganization of microtubules on wheat and *A. thaliana* (Chaimovitsh et al., 2011) and reduced cell division in *A. thaliana* roots, causing disorganization of root cells and altering the hormonal balance of auxin and ethylene in *Arabidopsis* seedlings (Graña et al., 2013b). Also, it caused

a decrease in the mitotic index in onion plants (Fagodia et al., 2017). Graña et al. (2020) reported that with just one-hour exposition to citral, *A. thaliana* seedlings showed 9000 genes strongly down-regulated in roots and 5500 in shoots. Moreover, *in silico* studies demonstrated that citral isomers (neral and geranial) can interact with many single-stranded DNA-binding proteins (SSBPs), causing a direct inhibition of gene transcription in *Arabidopsis* treated seedlings (Graña et al., 2020).

Farnesene (Fig. 1) is a widely distributed sesquiterpene involved in both plant- and insect-communication (Vourinen et al., 2003), which has also shown phytotoxic potential in altering the root growth of *A. thaliana* seedlings (Araniti et al., 2013).

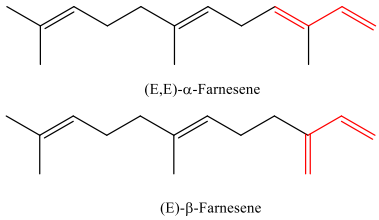

Figure 1. Farnesene's alpha (up) and beta (down) stereoisomers. The double bond position that differentiates the stereoisomers is shown in red.

Farnesen causes an increase in auxin and ethylene levels and stimulates oxidative damage through the production of NO, H_2O_2 and O_2^-, causing disruption of mitotic and cortical microtubules and inducing ultra-structural cell malformations that alter root growth of *A. thaliana* and remember those of citral (Araniti et al., 2016). Later, Araniti et al. (2017a) demonstrated that the microtubule disruption was a consequence of an altered auxin distribution caused by a farnesene-induced downregulation of the expression of all the auxin polar transport PIN proteins, accompanied by a degradation of the proteins PIN4 and PIN7, at the level of the quiescent center. Although the MOA of farnesene has not been studied so profoundly as citral, many of the effects observed for both compounds are highly similar (morphological alterations in the root, malfunction of microtubules, altered auxin balance, etc.), suggesting the possibility of shared action pathways for both terpenoids. Moreover, a visual comparison of neral and farnesene reveals a high structural similarity since the 1,5-octadienyl chain is present in both structures, which could determine their mode of action. Furthermore, there are already synthetic herbicides with a different chemical structure that affect the same molecular target, e.g., glyphosate and imazaquin (Gaines et al., 2020), which suggest that even with different chemical structures two natural compounds could share one or more target sites of action. Citral and farnesene are Generally Recognized

as Safe (GRAS) food additives by the US Food and Drug Administration. Moreover, it was demonstrated that farnesene acts as a neuroprotective agent against hydrogen peroxide-induced neurotoxicity *in-vitro* and could be used as an antioxidant compound resource that may have applications in the food and drug industries (Çelik et al., 2014).

Therefore, independent metabolomic studies of *A. thaliana* seedlings treated at two different times (24 and 48 h) with the IC_{50} of citral and farnesene were done, together with *in silico* studies of the interaction of farnesene with the single-stranded DNA-binding proteins (SSBPs) and the comparison of the binding sites of farnesene with those previously found for citral (Graña et al., 2020). Farnesene is a mixture of six unsaturated sequiterpenes, among which the alpha and beta stereoisomers differ in the arrangement of the conjugated double bonds (Fig. 1). The (3E,6E)-3,7,11-trimethyldodeca-1,3,6,10-tetraene, namely (E,E)-α-farnesene isomer, is the most widespread in nature. However, there can be more than four alpha geometric stereoisomers in two of its three internal double bonds. Furthermore, the (E,E)-α-farnesene structure has two methylene bridges that provide conformational flexibility. To study the putative molecular mechanisms of farnesene as a potential bioherbicide and to compare these results to those previously found for citral (Graña et al., 2020), its binding affinities to different transcription factors (AtWHY-2, ANAC and SHR-SCR complex) were calculated with ICM docking approaches.

In addition, parameters related to the PSII photosynthetic performance of plants treated with citral and farnesene were also studied in a short-term experiment on *Arabidopsis* seedlings at the same measuring times as the metabolomics study to investigate the mechanism of action of these two specialised metabolites and to compare whether they have similar modes of action on the photosynthetic process. A sensitive imaging fluorometer technique was adopted as a fast-screening method to effectively compare *in-vivo* the effects of these two terpenoids on seedling performance.

MATERIALS AND METHODS

Plants growth conditions

Arabidopsis thaliana (L.) Heynh. ecotype Columbia (Col-0) seeds were sterilised and vernalized as previously described by Araniti et al. (2016) and sown (24 seeds per replicate) in square Petri dishes (100 x 150 mm) filled with plant agar (0.8% w/v) enriched with micro- and macro-nutrients (basal salt-medium Murashige-Skoog, Sigma-Aldrich) and supplemented with 1% sucrose (pH 6.0). The plates were placed, vertically for metabolomic studies or horizontally for chlorophyll *a* fluorescence measurements, in a growth chamber at 22 ± 2 °C, 55% relative humidity and a short-day photoperiod with 8 daylight

hours (75 μmol $m^{-2}s^{-1}$) and 16 h darkness. Plants were left to grow for 14 days. After this time, 4 mL of the IC_{50} (323 μM, Araniti et al., 2013) of farnesene (Sigma-Aldrich) or the IC_{50} (194 μM, Graña et al., 2013b) of citral (Sigma-Aldrich) were added to each plate. The compounds were diluted in 0.1% ethanol as solvent (control plates included 0.1% EtOH, too). Then, plates were incubated horizontally for 24 and 48 h. Although previous gene expression and *in-silico* studies were done with citral for 1 to 24 h (Graña et al., 2020), the measuring times used in this work for comparison of citral and farnesene effects were set up at 24 and 48 h to allow protein codification, enzymatic reactions and metabolites' synthesis as a consequence of these first observed effects for citral.

Chlorophyll *a* fluorescence measurements

The imaging fluorometer was used during the experiments as a screening tool since the primary phytotoxic effects of a specific toxin can be quickly monitored *in-vivo* on the same plant, and the effects are visible even before macroscopic alterations such as chlorosis, necrosis or growth reductions can be detected (Sánchez-Moreiras et al., 2020). The chlorophyll *a* fluorescence emitted by plants (four seedlings per treatment and time) was determined as described by Graña et al. (2013b) with a Maxi-Imaging-PAM fluorometer (Walz, Effeltrich, Germany) after 0, 24 and 48 hours of treatment with IC_{50} of farnesene and citral. This apparatus gives all the parameters related to the measurement of chlorophyll *a* fluorescence, and takes pictures of this fluorescence to obtain a view of the photosynthetic activity of the entire plant and its spatio-temporal variations over time (Martínez- Peñalver et al., 2011; Sánchez-Moreiras et al., 2020). The plants were kept in darkness for 10 min to open all the reaction centers. After this time, seedlings were successively illuminated at 0.5 $\mu mol \cdot m^{-2} \cdot s^{-1}$ to measure the initial fluorescence (F_0). Then a saturating pulse of 2700 $\mu mol \cdot m^{-2} \cdot s^{-1}$ was used to measure the maximum fluorescence of dark-adapted seedlings (F*m*). After five minutes of actinic illumination at 120 $\mu mol \cdot m^{-2} \cdot s^{-1}$ (with measurement of the corresponding fluorescence, F_s), samples received 20 s of 800-ms saturating pulses of 200 $\mu mol \cdot m^{-2} \cdot s^{-1}$ to assess the maximum fluorescence of light-adapted leaves (F*m*'). These values were used to calculate the parameters used for comparisons between treatments: maximum quantum efficiency of dark-adapted photosystem II (F*v*/F*m*); quantum efficiency of photosystem II (Φ_{II}); energy dissipation in the form of heat (Φ_{NPQ}); non-regulated energy dissipation (Φ_{NO}, fluorescence emission); and the estimated electron transport rate (ETR) (Kramer et al., 2004; Klughammer and Schreiber, 2008). The photosynthetic response was monitored for 5 min, and fifteen measurements were obtained for each parameter.

Extraction, identification and quantification of primary metabolites

Extraction, derivatisation, identification, and quantification of metabolites from *Arabidopsis* shoots treated for 24 and 48 h with citral or farnesene (IC_{50}) were performed, as reported by Lisec et al. (2006). The derivatised extracts were injected into a gas chromatograph apparatus (Thermo Fisher G-Trace 1310) coupled to a single quadrupole mass spectrometer (ISQ LT). Samples chromatographic separation was achieved using a capillary column TG-5MS 30 m×0.25 mm×0.25 µm and helium (6.0) as carrier gas.

The injector and source were settled at 250 °C and 260 °C, respectively. One µL of the sample was injected in splitless mode with a flow of 1 mL min^{-1}. The programmed temperature was settled as follows: isothermal at 70 °C for 5 min followed by a 5 °C/ min ramp to 350 °C and final heating at 330 °C for 5 min. Mass spectra were recorded in electronic impact (EI) mode at 70 eV, scanning at 45–600 m/z range. Chromatographic alignment, deconvolution, intensity extraction and peaks annotation were carried out using the open source software MS-DIAL. The average peak width of 20 scans and a minimum peak height of 1000 amplitudes was applied for peak detection. The sigma window value was 0.5 and EI spectra cut-off of 10 amplitudes was implemented for deconvolution. For peaks identification, the retention time tolerance was settled at 0.5 min, the m/z tolerance at 0.5 Da, the EI similarity cut-off was 70%, and the identification score cut-off was 70%. In the alignment parameters setting process the retention time tolerance was settled to 0.075 min. Metabolites annotation was achieved using an in-house library built with publicly available MS spectra, as Misra (2019) reported.

Metabolites identification was made following the metabolomics standards initiative guidelines (MSI) for metabolite identification (Sansone et al., 2007). In particular, features were annotated at Level 2 [identification based on the spectral database (match factor >70%)] and Level 3 [identification based on the spectral database (match factor >70%)]. Relative metabolites normalization was based on an internal standard (ribitol at 0.02 mg mL^{-1}), added during the extraction process (Lisec et al., 2006).

***In silico* studies**

Molecular modelling studies

Flexible ICM (Internal Coordinate Mechanics software) docking was used to optimize the internal coordinates of the farnesene located in the protein pocket. Previously, conformational analysis was performed outside the protein pocket, and low-energy conformations were used as initial geometries for docking. Ligand binding modes were scored according to the farnesene-target complex results and ranked using the full ICM scoring function. A low ICM score suggests favourable ligand-protein binding

affinity. The scoring function was calculated as the weighted sum of the following parameters (Shapira et al., 1999): internal force-field energy of the ligand, entropy loss of the ligand between bound and unbound states, ligand-receptor hydrogen bond interactions, polar and non-polar solvation energy differences between bound and unbound states, electrostatic energy, hydrophobic energy, and hydrogen bond donor or acceptor desolvation.

Receptor Preparation

All proteins were prepared using the default ICM (Internal Coordinate Mechanics) settings (Abagyan and Totrov, 1994). The Protein Data Bank (PDB) crystal structures of AtWHY-2 (PDB code 4KOP: 1.8Å resolution); ANAC (PDB code: 1ut7: 1.9 Å resolution); and SHR-SCR complex (PDB code 5b3g: 2 Å resolution) proteins from *Arabidopsis thaliana* were converted to ICM objects.

Ligand preparation

α-Farnesene structure (PubChem CID 5281516) and citral (PubChem CID 643779) were imported into ICM, converted to 3D structure, and all conformers were calculated, i.e. to generate 3D series of conformers for both ligands, a maximum number of conformations of 30, an effort value of 10 and a thoroughness of 10 were calculated. Farnesene and citral molecules were first subjected to conformational analysis outside the protein pocket using the MMFF force field. Low energy conformations were collected and used as starting geometries for protein-ligand docking.

Molecular docking

α-Farnesene and citral were placed into WHY-1, WHY-2, WHY-3 proteins from the Whirly family (Protein Data Bank, PDB code 4KOO: 1.9 Å resolution; 4KOP: 1.8 Å resolution; 4KOQ 1.9 Å resolution); ANAC from the NAC family (PDB code: 1ut7: 1.9 Å resolution); SHR-SCR complex from the GRAS family (PDB code 5b3g: 2 Å resolution), and MYC2 tetrameric from the bHLH family (PDB code 5GNJ: Resolution: 2.7 Å resolution) from *A. thaliana*, and docking poses were scored by scoring functions according to their most energetically favourable protein binding conformation, using ICM flexible docking method (Abagyan et al., 1994).

Statistical analysis

A completely randomised design with four replicates was applied in all the experiments. Chlorophyll fluorescence parameters were analysed through one-way ANOVA using Tukey's test as

post-hoc ($p \leq 0.05$). Metabolite concentrations were checked for integrity, and missing values were replaced by a small positive value (half of the minimum positive number detected in the data). Data were successively normalised by a reference sample (ribitol), transformed through "Log normalisation" and scaled through Auto-Scaling. Data were then classified through unsupervised Principal Component Analysis (PCA) to get the score plot (to visualise group discrimination) and the loadings plot (to identify metabolites contributing to groups separation). The data were further analysed through the supervised Partial least-squares discriminant analysis (PLS-DA). Features selection, with the highest discriminatory power, was based on their variable importance in projection (VIP) score > 1. To avoid overfitting, the PLS-DA model was validated using Q2 as a performance measure, the 10-fold cross-validation and setting in the permutation test a permutation number of 20 (see figures reported in Supplementary Table S1-PLSDA loadings).

Data were then analysed through the univariate analysis one-way ANOVA using the LSD test as post-hoc ($P \leq 0.05$) to highlight statistical differences among single metabolites and treatments. A false discovery rate was applied to the nominal *p*-values as a control for false-positive findings. All the features significantly affected by the treatments (in the ANOVA test) were presented as a heatmap and clusterised using the Euclidean method for distance measurement and the Ward algorithm for group clusterisation. Further, a Student's *t*-test analysis ($P \leq 0.05$) was carried out for each time of exposure (24hr and 48hr) to identify potentially different metabolites affected by the treatments.

Finally, a pathway analysis was performed with MetPA, a web-based tool that combines results from pathway enrichment analysis and topology analysis, which allowed the evaluation of the possible biological impacts on the perturbed pathways (Araniti et al., 2017b). All the metabolomics analyses were carried out using Metaboanalyst 3.0 (Xia et al., 2015). All the raw and analysed metabolomic data are reported in supplementary material, Table S1.

RESULTS

Many similarities, but also some differences, could be detected among citral and farnesene treatments when looking at the metabolomic variations in *Arabidopsis* seedlings treated with both compounds after the same measuring times than those of fluorescence emission. In order to assess the influence of the treatments on overall metabolites, raw data were analyzed through principal component analysis (PCA) for the 67 compounds identified by GC-MS analyses (Table 1).

Table 1. The annotated and relatively quantified chemical compounds significantly affected after the exposition to farnesene (323 µM) and citral (194 µM) for 24 or 48 h.

Molecules	F24	F48	C24	C48	
	t.stat				
Beta-Alanine	//	**-3.531**	//	**-8.804**	**Aminoacids**
GABA	//	**-4.744**	**-19.11**	**-7.152**	
Glycine	//	13.82	//	6.843	
L-Alanine	//	//	**-5.845**	**-5.041**	
L-Asparagine	//	//	//	**-6.202**	
L-Aspartic acid	//	//	23.71	14.18	
L-Glutamic acid	//	**-3.732**	//	7.845	
L-Glutamine	//	**-7.970**	**-6.360**	**-10.39**	
L-Lysine	**-12.65**	**-5.453**	**-10.33**	**-4.094**	
L-Proline	//	//	**-4.866**	**-14.09**	
L-Serine	**-5.795**	**-7.698**	**-7.989**	**-18.65**	
L-Threonine	//	**-9.210**	**-8.083**	**-6.791**	
Pyroglutamic acid	//	//	//	**-3.410**	**Amino acid derivative**
Cadaverine	**-4.076**	**-8.558**	**-18.45**	**-17.07**	**Polyamines**
Citrulline	**-4.368**	**-5.678**	//	**-4.341**	
Ornithine	//	**-3.668**	**-6.984**	**-4.671**	
Putrescine	**-13.06**	**-19.95**	**-11.96**	**-13.48**	
2-Keto-D-gluconic acid	//	**-6.651**	**//**	**-6.829**	**Organic acids**
Citric acid	**-4.684**	//	//	5.731	
Oxalic acid	//	//	//	7.516	
Oxoglutaric acid	//	//	//	10.85	
Glutaric acid	//	//	**-6.247**	//	
Glyceric acid	9.608	5.935	//	6.549	
Glycolic acid	//	//	**-4.234**	//	
Pyruvic acid	//	4.737	3.193	8.272	
Propionic acid	//	//	**-5.894**	//	
Succinic acid	//	6.342	5.724	6.434	
Threonic acid	//	**-8.160**	**-3.378**	**-10.99**	
Allose	//	**-10.99**	//	//	**Sugars**
Alpha-Lactose	**-16.84**	**-9.342**	**-17.56**	**-11.09**	
Erythrose	//	//	5.247	3.395	
D-Glucose	//	//	//	3.802	
Sucrose	8.780	6.320	5.070	5.239	
Turanose	3.836	//	//	4.291	
Myoinositol	//	//	**-5.127**	//	**Sugar alcohol**
Sinapic acid	//	//	5.856	6.918	**Phenolic acids**
Benzoic acid	//	21.50	//	22.61	
Palmitelaidic acid	//	**-5.695**	9.301	//	**Fatty acids**
Dodecanoic acid	//	//	44.97	**-4.357**	
Decanoic acid	//	//	//	**-13.08**	
Adipic acid	//	6.782	//	2.929	
3-Indoleacetonitrile	//	//	11.44	6.593	**Miscellaneous**
Phosphoric acid	**-6.333**	**-11.65**	**-7.913**	**-6.886**	
Urea	11.08	3.876	8.733	6.069	
N-Alpha-acetyllysine	**-4.353**	**-10.16**	**-10.34**	**-14.26**	

Important features selected by t-tests with threshold $p \leq 0.05$. Negative t-stat values indicate up-accumulated metabolites, whereas positive t-stat indicates down-accumulated metabolites. //: Not Significant features. Data are expressed in nanograms/100 mg of fresh plant material. N=4.

The score plot of the unsupervised PCA (Fig. 2a) highlights the separation between control and treatments. The grouping observed during PCA analysis was further confirmed by cluster analysis (Fig. 2d), which pointed out the formation of two main separated groups (control and treatments), being citral and farnesene grouped in the same cluster branch at the higher level and in separated units at a lower level (Control, Farnesene and Citral) (Fig. 2d). The supervised PLS-DA analysis (Fig. 2b) confirmed the separation, previously observed with the PCA, characterized by three separated groups (control, citral and farnesene), which were distributed in three different quadrants. Interestingly, while both farnesene samples (24 and 48 h) were grouped, citral treatments were separated, indicating a stronger effect of citral when increasing the time of exposure (Fig. 2a). The separation was achieved by virtue of the first two principal components (PCs) PC1 *vs* PC2, which explained a total variance of 45%. PC1 explained the highest variance (31%), while PC2 explained the 14% of the total variance. The PCA loading plot highlighted that PC1 was dominated by putrescine, N-α-acetyllysine, cadaverine, L-threonine, serine, sucrose and glyceric acid, whereas PC2 was dominated by glutamic, fumaric, citric, malic, decanoic and propionic acids, and alanine (supplementary material, Table S1). Moreover, the VIP score analysis pointed out that several sugars, polyamines and amino acids were the classes of compounds mainly contributing to groups discrimination (Fig. 2c). In particular, the treatments with citral induced, at both times of treatment (24 and 48 h), a significant accumulation of phosphoric acid, L-lysine, citrulline, ornithine, putrescine, cadaverine and threonic acid, and a reduction in glucose, pyruvic acid, fructose, urea, sucrose, and glycine (Fig. 2c). A similar trend was also followed by farnesene, which induced increments and decrements of the same metabolites affected by citral even when the differences were less marked (Fig. 2d).

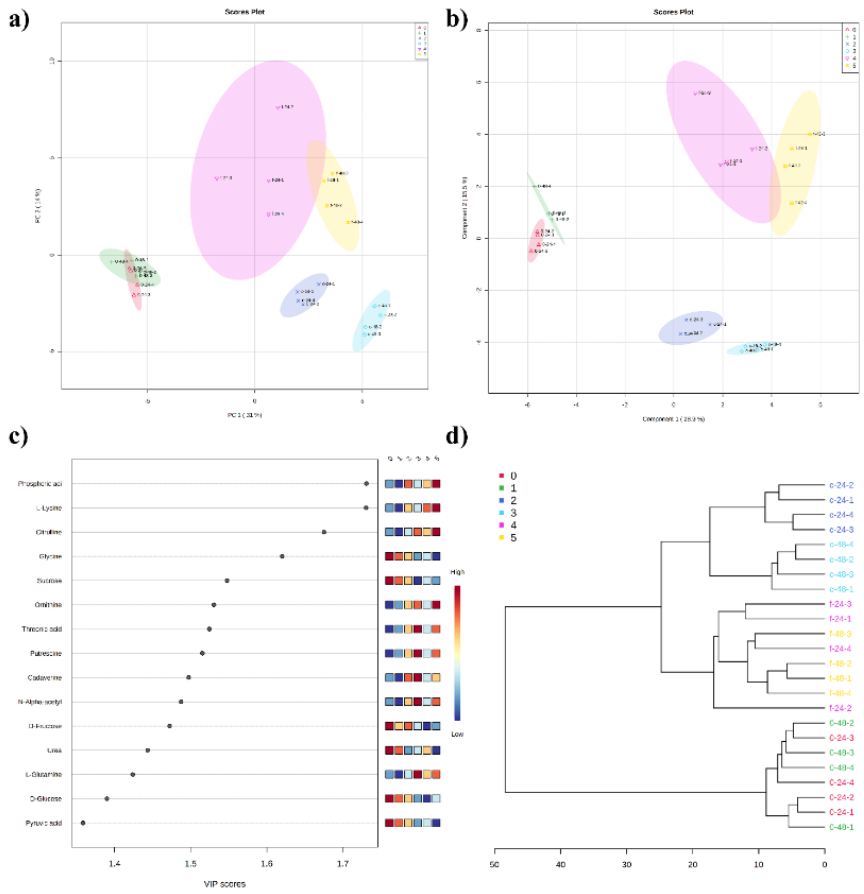

Figure 2. PCA (a), PLS_DA (b-c) and cluster analysis (d) carried on the metabolite identified and quantified after farnesene (323 µM) and citral (194 µM) treatments. a) PCA scores plot between the selected PCs; b) PLS-DA scores plot between the selected PCs, the explained variances of PCA and PLS-DA are shown in brackets; c) Important features identified by PLS-DA. The coloured boxes on the right indicate the relative concentrations of the corresponding metabolite in each group under study; d) Clustering result shown as a dendrogram (distance measure using euclidean, and clustering algorithm using ward. D). 0-24 (0, ▲ or red colour) and 0-48 (1, + or green colour) indicate control replicates after 24 and 48 h, respectively; C-24 (2, X or dark blue) and C-48 (3, ○ or light blue) indicate citral replicates after 24 and 48 h; F-24 (4, ▼ or magenta) and F-48 (5, □ or yellow) indicate farnesene replicates after 24 and 48 h, respectively, respectively. N=4.

The univariate ANOVA analysis revealed that 40 out of the 67 compounds identified were significantly altered among both treatments (supplementary material, Table S1). Those 40 metabolites were reported on a heatmap, which gave an overview of the trend of each metabolite among the treatments and times of exposition (Fig. 3). Finally, a t-test analysis was carried out comparing each treatment at a given time of treatment (24 or 48 h) with its relative control (24 or 48 h) and the results were reported in Table 1. The analysis highlighted that in total 45 metabolites out of 67 were affected by the treatments. In particular, after 24 h, only 28 and 13 metabolites were affected by citral and farnesene respectively, whereas at 48 h, 39 and 26 metabolites were respectively affected. Interestingly, when we compare 24 h treatment of citral with 24 h farnesene, just nine metabolites were found to be commonly affected, while when comparing 48 h citral with 48 h farnesene, there were up to 22 metabolites commonly affected. Notably, most amino acids and polyamines increased their levels between treatments, while sugars decreased, except for alpha lactose and allose, which increased. As for organic and fatty acids and miscellaneous compounds, some of them increased while others decreased, whereas phenolic acid levels were reduced between treatments (Table 1 and supplementary material, Table S1).

Finally, a detailed analysis concerning the pathways affected by farnesene and citral treatments was performed using the metaboanalyst module "MetPa". The pathway analysis of the results allowed identifying treatment impact on plant metabolism. In general, farnesene and citral similarly affected the same pathways after 48 h of treatment, whereas the exposure to both molecules for 24 h highlighted that citral was more rapid than farnesene in affecting those pathways (Table 2). In particular, 20 pathways were significantly affected by citral and farnesene treatments, but only 11 had an impact score higher than 0.20. The three routes with a pathway impact score higher than 0.50 were alanine, aspartate and glutamate metabolism, beta-alanine metabolism, and glycine serine and threonine metabolism, pathways related to amino acid metabolism (Table 2 and supplementary material, Table S1).

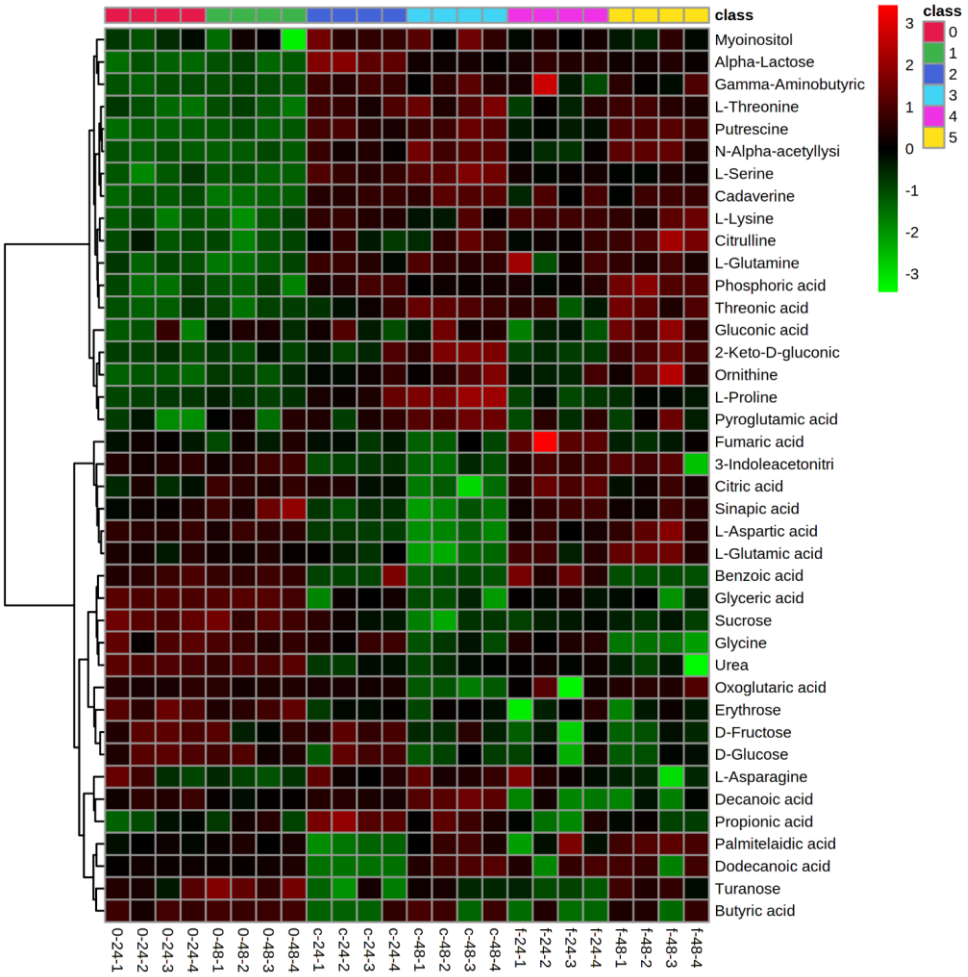

Figure 3. Overlay heat map of the 40 metabolites resulted from the ANOVA test (LSD $p \leq 0.05$ and FDR ≤ 0.05) significantly altered in seedlings exposed to farnesene (323 µM) and citral (194 µM) for 24 and 48 h. Each square represents the effect of farnesene and citral on the amount of every metabolite using a false-colour scale. Dark red or dark green colors respectively indicate an increase or decrease in metabolite content. 0-24 (class 0) and 0-48 (class 1) indicate control replicates after 24 and 48 h, respectively; C-24 (class 2) and C-48 (class 3) indicate citral replicates after 24 and 48 h; F-24 (class 4) and F-48 (class 5) indicate farnesene replicates after 24 and 48 h, respectively. N=4.

Table 2. Results from ingenuity pathway analysis with MetPa carried out on *Arabidopsis* seedlings treated with farnesene (323 µM) and citral (194 µM) for 24 and 48 h.

Pathways	Total Cmpd	Hits	Farnesene 24		Farnesene 48		Citral 24		Citral 48		Impact
			Raw p	-LOG(p)	Raw p	-LOG(p)	Raw p	-LOG(p)	Raw p	-LOG(p)	
Alanine aspartate and glutamate metabolism	22	10	//	//	0.0005	75.981	1.04E-01	11.472	7.17E-03	14.149	0.87
beta-Alanine metabolism	12	2	//	//	0.0046	53.719	//	//	1.44E-04	18.054	0.54
Glycine serine and threonine metabolism	30	5	0.0022	6.1010	2.41E-01	10.631	1.97E-04	15.442	4.79E-03	14.551	0.53
Galactose metabolism	26	6	1.08E-02	11.432	0.0001	91.322	1.35E-02	13.517	0.0001	8.9770	0.47
Arginine and proline metabolism	38	10	7.16E-01	95.446	1.74E-01	10.959	8.52E-05	18.581	1.23E-05	18.216	0.41
Citrate cycle (TCA cycle)	20	6	//	//	2.86E-01	10.462	0.0115	44.682	1.20E-02	13.629	0.28
Glyoxylate and dicarboxylate metabolism	17	4	0.0307	34.849	0.0104	4.5700	0.0050	52.996	0.0010	69.274	0.27
Inositol phosphate metabolism	24	1	0.0136	43.009	//	//	0.0022	61.361	//	//	0.25
Tryptophan metabolism	27	1	//	//	//	//	2.68E-02	10.527	0.0006	74.437	0.21
Pantothenate and CoA biosynthesis	14	3	//	//	1.11E-02	11.405	//	//	2.24E-02	13.010	0.20
Pyruvate metabolism	21	3	//	//	0.0002	85.275	//	//	0.036685	33.054	0.20
Methane metabolism	11	2	9.04E-02	11.614	3.06E-02	12.699	4.68E-01	99.692	1.01E-03	16.104	0.17
Glycolysis or Gluconeogenesis	25	2	//	//	0.0007	72.245	//	//	0.0128	43.602	0.11
Aminoacyl-tRNA biosynthesis	67	11	//	//	1.61E-01	11.035	2.60E-03	15.163	8.41E-05	18.594	0.09
Starch and sucrose metabolism	30	3	0.0019	62.883	0.0043	54.468	0.0014	65.971	0.0027	59.048	0.09
Glutathione metabolism	26	5	0.0025	59.886	5.41E-03	14.431	5.26E-02	12.156	4.32E-04	16.956	0.09
Lysine biosynthesis	10	2	3.47E-01	10.270	0.0027	59.141	1.77E-03	15.546	6.93E-02	11.879	0.07
Phenylpropanoid biosynthesis	45	1	0.0469	30.595	//	//	0.0011	68.164	0.0005	7.7030	0.04
Carbon fixation in photosynthetic organisms	21	4	//	//	0.0027	59.043	0.0002	83.857	7.46E-02	11.807	0.03
Valine leucine and isoleucine biosynthesis	26	3	//	//	0.0001	9.1770	0.0005	75.641	8.20E-02	11.711	0.02
Purine metabolism	61	2	0.0032	5.7450	0.0006	74.136	0.0001	9.1350	7.63E-01	94.807	0.01

Total Cmpd: the total number of compounds in the pathway; Hits: is the matched number from the uploaded data; P value: is the original *p* value calculated from the enrichment analysis; Impact: is the pathway impact value calculated from pathway topology analysis. //: not significantly impacted pathways. N=4.

If we look at the results obtained from the measurement of chlorophyll *a* fluorescence, all parameters related to this measurement were affected by both treatments, IC_{50} farnesene and citral (Fig. 4), at the two treatment times of exposure (24 and 48 h). Farnesene and citral significantly reduced the photochemical quenching (Φ_{II}). The Φ_{II} value in control was 4.48 A.U. after 48 h, while in citral and farnesene treatments the values were 1.75 and 2.57 A.U., respectively. Both compounds caused a significant increase in heat energy dissipation (Φ_{NPQ}, from 2.46 A.U. in control to 6.04 and 4.02 A.U. in citral and farnesene treatments) and non-regulated energy emission as fluorescence (Φ_{NO}, from 5.06 A.U. in control to 7.69 and 7.29 A.U. in citral and farnesene respectively). However, farnesene-treated plants were most able to maintain high levels of regulated energy emission (Φ_{NPQ}) than citral-treated plants after 48 h of treatment

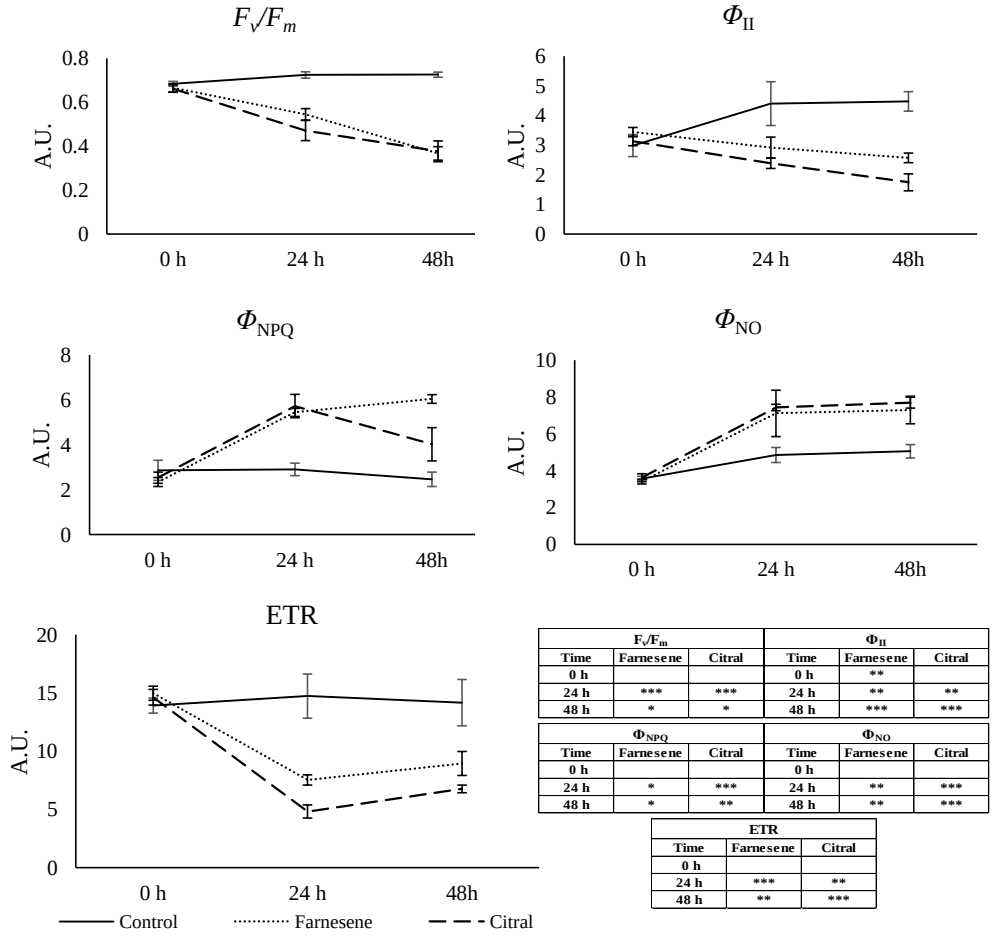

F_v/F_m		
Time	Farnesene	Citral
0 h		
24 h	***	***
48 h	*	*

Φ_{II}		
Time	Farnesene	Citral
0 h	**	
24 h	**	**
48 h	***	***

Φ_{NPQ}		
Time	Farnesene	Citral
0 h		
24 h	*	***
48 h	*	**

Φ_{NO}		
Time	Farnesene	Citral
0 h		
24 h	**	***
48 h	**	***

ETR		
Time	Farnesene	Citral
0 h		
24 h	***	**
48 h	**	***

Figure 4. Values of the maximum quantum efficiency of dark-adapted PSII (F_v/F_m), the effective photochemical quantum yield of the light adapted PSII Φ_{II}, the quantum yield of light induced nonphotochemical quenching Φ_{NPQ} (mainly heat), the chlorophyll fluorescence Φ_{NO},

and the apparent electron transport rate (ETR) in *Arabidopsis* seedlings treated at 0, 24 and 48 h with IC_{50} farnesene and IC_{50} citral. Control treatment represents untreated seedlings. Asterisks indicate significant * $p < 0.05$; very significant ** $p < 0.01$; and highly significant *** $p < 0.001$ differences when compared to the control. AU = Arbitrary Units. N = 4.

The Φ_{NO} images (Fig. 5) show how both treatments can similarly damage the cells close to the vascular bundles already 24 h after the treatment, and this effect was stronger with both compounds after 48 h of treatment. The electron transport rate (ETR) was also significantly reduced in both treatments at both times. At 48 h, there was a decrease from 14.15 A.U. in control to 6.78 and 8.95 A.U. in citral and farnesene, respectively. Finally, the maximum efficiency of PSII dark-adapted system (F_v/F_m) was significantly reduced, from 0.73 A.U. in control to 0.38 and 0.37 A.U. in citral and farnesene, respectively, after 48 h of treatment. As shown in the F_v/F_m image (Fig. 5), this parameter was reduced in the center of the rosette at 24 h of treatment. Successively, this reduction extended to the rest of the seedling shoot after 48 h of treatment.

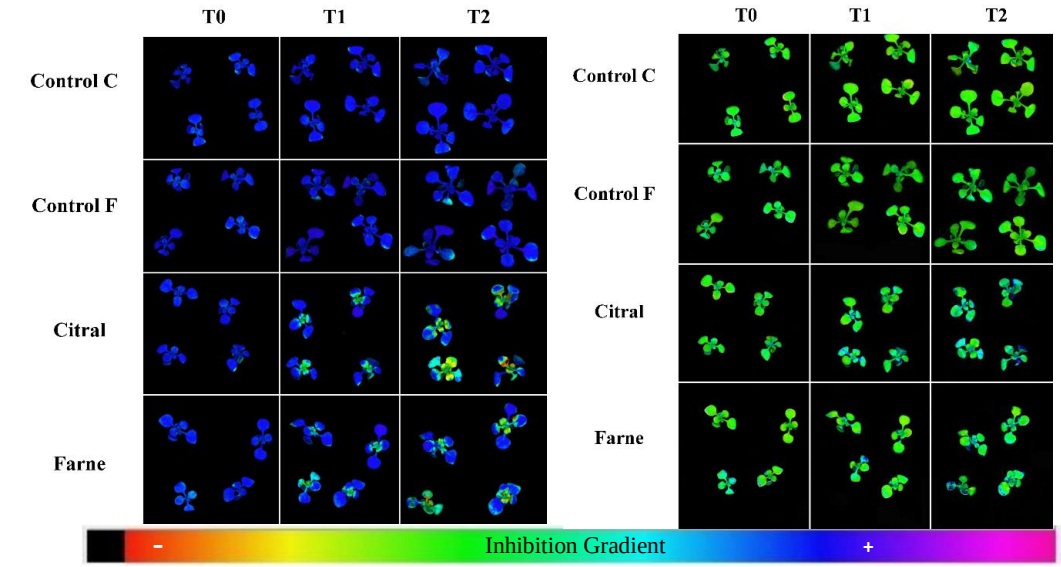

Figure 5. Pseudo-color images of dark-adapted PSII (*Fv/Fm*) (left) and of non-regulated energy emission as fluorescence (Φ_{NO}) (right) in *Arabidopsis* seedlings after farnesene and citral exposition. Images were taken at the beginning (T0) and at 24 (T1) and 48 h (T2) of treatment. Images of the different fluorescence parameters are depicted in false colors coding from 0.0 (black) to 1.0 (purple). N= 4.

In parallel, a comparative study between farnesene and *cis*-citral isomer (also known as neral) was also done in *in silico* studies (farnesene *vs* citral) for DNA binding proteins on transcription factors previously found to be altered by citral (Graña et al., 2020). Table 3 shows that WHY-1, WHY-2, WHY-3, MYC-2 and NAC-1 were characterized by a very similar binding energy value for farnesene and citral, while different values were obtained when testing SHR_SCR.

Table 3. Binding energy scores between farnesene and citral on six different transcription factors (WHY-1, WHY-2, WHY-3, NAC, MYC and SHR-SCR) in ICM-docking studies. Nflex is the number of rotatable torsions; Eintl is internal conformation energy of the ligand; SolEl is the solvation electrostatics energy change upon binding; dTSc is the loss of entropy by the rotatable protein side-chains; Hbond is Hydrogen Bond energy.

PROTEIN	LIGAND	Score	Nflex	Eintl	SolEl	dTSsc	Hbond
WHY-1	Farnesene	-23.09	5	4.84	1.73	0.27	-
WHY-1	Neral	-23.40	3	1.93	5.65	0.81	-5.53
WHY-2	Farnesene	-20.33	5	1.16	1.51	1.04	-
WHY-2	Neral	-17.09	3	1.14	0.75	0.97	-1.92
WHY-3	Farnesene	-18.48	5	4.69	1.96	0.60	-
WHY-3	Neral	-20.85	3	2.63	1.92	0.56	-4.72
NAC-1	Farnesene	-18.48	5	3.60	6.86	1.11	-
NAC-1	Neral	-17.11	3	1.28	3.04	0.76	-2.23
MYC-2	Farnesene	-14.88	5	5.00	2.41	1.85	-
MYC-2	Neral	-19.26	3	3.68	3.15	0.94	-4.50
SHR_SCR	Farnesene	-15.70	5	4.60	3.42	1.48	-
SHR_SCR	Neral	-22.00	3	1.93	3.43	0.22	-4.44

As Graña et al. (2020) showed the interaction of the complex AtWHY-2-neral (cis isomer of citral) is the most effective, with spatial proximity between the ligand and two of the amino acids involved in binding to a specific ssDNA fragment (His 136 and Asp 137), which could effectively avoid the interaction between the amino acids WHY-2 and ssDNA, the *in silico* comparison of the effects of farnesene *vs* citral on this transcription factor was more deeply studied (Table 4). ICM Molecular modelling, carried out between AtWHY2 and farnesene or citral (Table 4), reported very similar results for both terpenoids. On

the contrary, as previously found with neral (Graña et al., 2020), farnesene is placed far from the union site with the DNA for AtWHY-1 and AtWHY-3, therefore not in-depth studies were done for these transcription factors in the present work.

Visual comparison of neral and farnesene reveals a high structural similarity, since the 1,5-octadienyl chain is present in both structures. Neral also possesses an aldehyde group that allows establishing hydrogen bonds with the side chains of the hydrophobic pocket residues, as shown in Table 4 (column N-HBond). However, the absence of a hydrogen bond acceptor oxygen atom in the polyene hydrocarbon structure of farnesene does not allow establishing this type of dipole-dipole interaction, which explains why the F-HBond values are all equal to 0. Table 4 also shows the interest of this comparison study between the two structures. Thus, in the farnesene structure, which presents a longer olefin, an increase in the contribution of the hydrophobic energy in the exposure of the ligand surface to water (F-Hphob column) and of the Vander waals interaction energies (F-VwInt column) is observed, maintaining good protein-ligand docking scores.

Table 4. ICM Molecular docking results of Farnesene (F) and Citral (N) on AtWHY2. Pose: protein-ligand binding sites; F-Score and N-Score = ICM scores; F-Hbond and N-Hbond = hydrogen bond energies; F-Hphob and N-Hphob = hydrophobic energies in exposing a surface to water; F-Vwint and N-Vwint = Vander waals interaction energies.

Pose	F-Score	N-Score	F-Hbond	N-Hbond	F-Hphob	N-Hphob	F-VwInt	N-VwInt
1	-20.33	-17.09	0.00	-1.92	-7.26	-4.94	-23.02	-16.58
2	-20.02	-16.67	0.00	-1.94	-7.31	-5.09	-22.95	-15.23
3	-19.08	-16.31	0.00	-1.82	-7.35	-4.50	-22.98	-17.36
4	-18.5	-15.84	0.00	-1.89	-7.32	-4.93	-21.89	-15.46
5	-18.49	-15.62	0.00	-1.86	-5.53	-4.68	-22.47	-15.96
6	-18.25	-15.13	0.00	-2.06	-7.08	-4.52	-23.03	-20.24
7	-18.2	-15.04	0.00	-1.36	-6.5	-4.93	-20.26	-16.95
8	-18.19	-14.72	0.00	-1.95	-7.21	-4.77	-22.85	-15.06

AtWHY2 is a whirly protein directed to mitochondria in *Arabidopsis* that has an assembled structure into a tetramer in solution (Cappadocia et al., 2013). This arrangement of protein chains results in a central hydrophobic pocket surrounded by residues, such as Phe198, Ala199, Pro201 or His202. The four lower-energy docked poses of farnesene on AtWHY2 in this binding site 1 (poses 1-4, table 4) could be

stabilized by hydrophobic interactions between its unsaturated alkyl chain and side groups of hydrophobic residues, which surround the central binding pocket, as can be seen in Fig. 6.

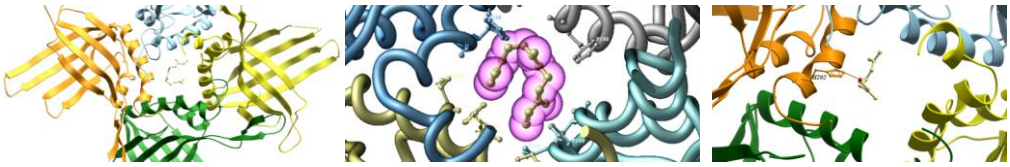

a b c

Figure 6. a) Farnesene structure (yellow) docked into the binding site of AtWHY-2 central hydrophobic pocket; b) volume area of farnesene and AtWHY2 residues less than 5A is shown; c) citral structure (yellow) docked into binding site 1 of AtWHY-2. Hydrogen bonds are shown as dotted orange lines.

At this same binding site 1, citral is also docked on AtWHY2 in an energetically favorable score (pose 5). The model further suggests the formation of a hydrogen bond between citral and a histidine residue (H_2O_2) that stabilizes the protein binding (Fig. 6b). However, the energetically more favorable binding pose 1 of citral is very similar to pose 5 (still energetically favorable) of farnesene at binding site 2 of the protein (Fig. 7a). In this binding site 2, farnesene shows a position slightly closer than citral to key residues for AtWHY2 (His136 and Asp 137), reported already in previous studies (Graña et al., 2020), suggesting a similar putative inhibition effect on WHY2-ssDNA binding (Fig. 7b).

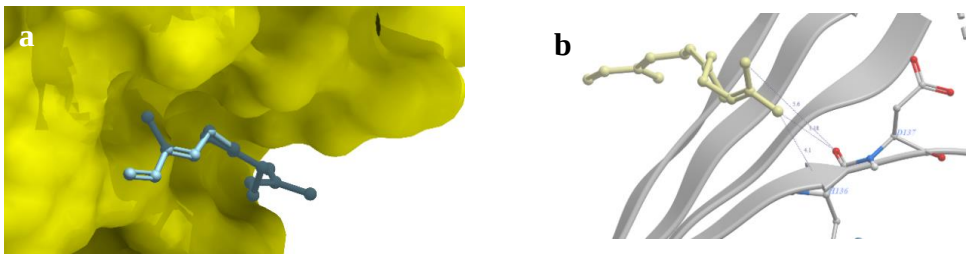

Figure 7. a) Pose 5 AtWHY2-Farnesene complex in binding site 2; b) proximity between farnesene (yellow) and two of the amino acids involved in binding to a specific ssDNA fragment (His 136 and Asp 137).

Regarding ANAC, other of the *in silico* studied binding proteins, it is interesting to highlight that the structure of the NAC domain is arranged as a dimer in solution (Ernst et al., 2004). Two saline bridges

formed by conserved Arg19 and Glu26 stand out among the residues involved in the union between dimers. In addition, an antiparallel beta-sheet is formed, cutting the dimer interface, with hydrogen bonds between Arg19…Arg19 and Tyr21…Gly17. In ICM molecular docking studies, all poses that energetically favor the binding of citral and farnesene metabolites on ANAC showed an arrangement of ligands at the binding site between NAC monomers. Citral has a hydrogen bond with a Gly17 residue (Fig. 8a), which stabilizes this pose; while farnesene is close to the antiparallel beta-sheet, specifically to Arg19 residue (Fig. 8b). Both ligands could make it challenging to stabilize the NAC dimer for ssDNA binding.

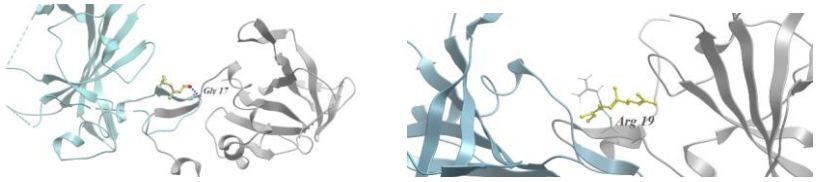

a) b)

Figure 8. a) Citral structure (yellow) docked into the binding site of NAC. Hydrogen bonds are shown as dotted green lines; b) Farnesene structure (yellow) docked into the binding site of NAC.

The comparative study of the effect on DNA binding proteins of farnesene *vs* neral (citral isomer) on SHR-SCR complex was also done. In this case, the comparative study between the ICM docking results of farnesene and citral against the SHR-SCR complex showed a different behaviour of both terpenes, as SHR-SCR-farnesene ICM docking results predicted a less favourable protein-ligand binding energy (Table 3). Furthermore, the interaction sites were very different in all poses. Similar results were obtained in the comparative study for the interaction of farnesene and neral with MYC-2, as neral showed better ICM docking than farnesene with score values of -19.26 and -14.88, respectively, and a hydrogen bound with the Lys 480 and Ser 479 residues (Fig. 9).

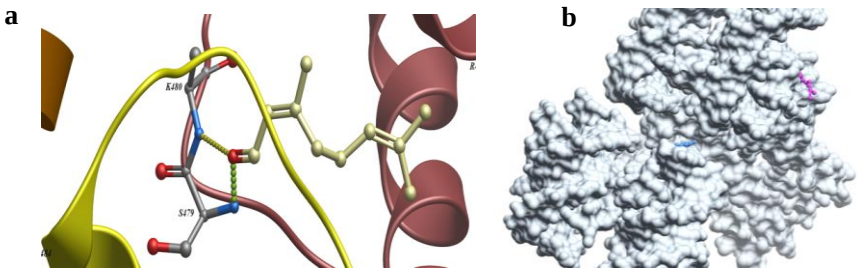

Figure 9. a) ICM-Pro docking model of neral (yellow) binding to MYC: hydrogen bonds are coloured as green and yellow dotted lines; b) ICM-Pro docking model binding of neral and farnesene to MYC in a toggle skin representation. Farnesene is coloured as pink and neral as blue.

DISCUSSION

The comparative metabolomics study revealed significant similarities but also differences between the two molecules. It is important to remember that the measuring times used in this work for comparing citral and farnesene effects were set up at 24 and 48 h to allow protein codification, enzymatic reactions and metabolites' synthesis as a a consequence of the effects observed with citral. If there are any errors during gene transcription, this could affect protein synthesis and enzyme activity in both roots and leaves. Regardless of the organ affected, these alterations could have consequences on functions performed by the plant, such as photosynthesis.

Both PCA and PLS-DA analyses, carried out on the annotated metabolites, highlighted a clear separation of the two molecules, which resided on two different quadrants. Also, the pathways analysis highlighted that both molecules were affecting similar pathways but to a different extent, as previously found for the fluorescence measurements.

The univariate analysis evidenced a clear similitude in the changes in concentration of specific compound classes. In particular, both terpenoids caused a decrease in most of the sugars, mainly glucose and sucrose, whose levels were significantly altered. The reduction of these sugars has been observed in *Arabidopsis* cells subjected to oxidative stress (Baxter et al., 2007) and in *Arabidopsis* roots isolated from seedlings treated with the natural compound rosmarinic acid (Araniti et al., 2018a). Low levels of sugars, especially the reduction in sucrose content caused by both compounds, might be due to the observed reduction in photosynthetic efficiency. Araniti et al. (2018b) observed that using *Origanum vulgare*

essential oils, whose composition is mainly based on the mixture of many terpenes, caused a reduction in photosynthetic efficiency and sucrose content, as observed in our assay. Sugar reduction could also have a side effect on the TCA cycle, one of the pathways affected by both compounds. Moreover, a reduction in pyruvate was observed in treated plants, which is known to be pivotal for the TCA cycle efficiency (Fernie et al, 2004).

The general decrease in sucrose content found in metabolomic analyses for both terpenoids after 24 and 48 h was the reason for performing chlorophyll *a* fluorescence, since it represents the main photosynthetic product.

The analysis carried out on treated seedlings showed that the PSII apparatus of *Arabidopsis* seedlings were similarly affected by both compounds and these effects were more significant after 48 h of treatment. The results indicated that the photosynthetic efficiency of PSII severely decreased for both compounds in treated seedlings, while a parallel increase of Φ_{NPQ} and Φ_{NO} was observed.

Φ_{NPQ} represents the fraction of energy dissipated via the regulated photoprotective NPQ (non-photochemical quenching) mechanisms in the form of heat [Δ-pH- and xanthophyll-regulated thermal dissipation; (Sánchez-Moreiras et al., 2020)]. The observed increment of this parameter after treatment with citral and farnesene suggests that excessive excitation energy can be efficiently dissipated into harmless heat and the PSII energy regulation mechanism. However, farnesene-treated plants maintained the the ability to dissipate the neregy in excess in the form of heat all over the treatment more than citral. In fact, the decrease of Φ_{NPQ} in 48 h citral-treated plants suggested that the plants cannot anymore compensate the excess of energy through a controlled energy emission Moreover, when plants were exposed to saturating light intensities, an increase of Φ_{NO} over Φ_{NPQ} reflected a suboptimal capacity of photoprotective reactions, eventually leading to photodamage and successively to chronic photoinhibition (Klughammer and Schreiber, 2008), as Φ_{NO} reflects the fraction of energy emitted mainly in the form of fluorescence as a consequence of closed PSII (Klughammer and Schreiber, 2008; Pfündel et al., 2008). For example, the previously described ability of these molecules to induce oxidative stress in *Arabidopsis* (Araniti et al., 2016; Graña et al., 2013) could be speculated to be a direct consequence of a reduced ability in processing light, probably due to an increase of close or damaged reaction centers, which leads to further ROS generation and propagation of oxidative stress, even at the level of chloroplast membrane.

Such ROS-guided phenomena are generally accompanied by a reduction of the dark-adapted PSII efficiency (F_v/F_m), significantly affected in our experiments, which indicates that the physiological status of the plant was altered, and a situation of photoinhibition or reduction of PSII activity is occurring

(Bresson et al., 2015). Looking at the images of F_v/F_m it is possible to observe that the citral- and farnesene-induced damages begin at the center of the rosette after 24 h of treatment and then extend to the rest of the shoot. This decrease may be a sign of physical damage to the PSII, as Graña et al. (2013a) observed. To protect the antenna complex in these situations, plants can dissipate excess energy through the previously described Φ_{NPQ} mechanism, which was strongly stimulated in our experiments, suggesting that plants treated can face stress in the short period. However, if the treatment time is prolonged, the harmful fluorescence energy emission (Φ_{NO}) is the predominant way of energy dissipation. This trend was highlighted and confirmed in the false color scale image of Φ_{NO} parameter, where a time-dependent stress progression can be observed. In addition, the alteration of the previously described parameters was accompanied by a reduction of the light-adapted PSII efficiency (Φ_{II}), confirming that plants were in a stress situation, and the energy dissipation mechanisms started to fail, especially faster in citral than in farnesene-treated plants (Kramer et al., 2004). These results are similar to the effects of the indole alkaloid norharmane assayed on adult plants of *A. thaliana* (López-González et al., 2020). Finally, the observed decrease in ETR might indicate failures in the biochemical phase of photosynthesis, such that electrons cannot reach their final acceptors (Oikonomou et al., 2019).

However, the pathways most affected by the treatments were related to amino acid metabolism, which significantly accumulated after molecules treatment to a different extent (more in citral-treated seedlings than in farnesene). Increases in amino acids such as GABA, proline or asparagine are related to stress resistance processes (Szabados and Savouré, 2009). In particular, proline can accumulate under oxidative stress to protect membranes and act as a scavenger of reactive species (Kishor and Sreenivasulu, 2014), while GABA levels increase under biotic and abiotic stress (Bouché and Fromm 2004). Another amino acid accumulated after treatments with a pivotal role in regulating cellular redox homeostasis under stress is glutamine (Ji et al., 2019), This accumulation of glutamine may be related to the observed urea reduction. The enzyme urease degrades urea to NH_3, which would be transformed with glutamate into glutamine by the action of the enzyme glutamine synthetase (GS) (Witte 2019). The observed increase in polyamines is also related to plant stress response (Podlešáková et al., 2019), and the increase in lysine and threonine levels is related to the synthesis of stress-specific proteins, as they are their typical components (Waters et al., 1996).

Moreover, the amino acid metabolic profiles obtained after citral and farnesene treatments were very similar to that observed on *Arabidopsis* plants treated with the terpenoid-alcohol nerolidol (Landi et al., 2020) and on lettuce plants exposed to the volatiles produced by the potentially allelopathic species *Dittrichia viscosa* (Araniti et al., 2017b). These results suggest that plants are experiencing oxidative

stress and are modulating their metabolism to face it, increasing the production of osmoprotectants (polyamine and quaternary ammonium compounds) and activating the previously described photoprotective mechanisms (Φ_{NPQ} and Φ_{NO}). In addition, a high accumulation of serine in plants was observed, which is an amino acid of great importance during the photorespiratory cycle (Bourguignon et al.,1998). Photorespiration is a process that, in stressful situations, can serve as an electron sink to maintain a correct flow of electrons and thus prevent oxidative damage (Osei-Bunsu et al., 2020). A negative correlation between photorespiration and ETR, as well as a positive correlation with proline content, has been observed under stress (Ünlüsoy et al., 2022). Thus, photorespiration would be activated after citral and farnesene treatment to compensate for the loss of photosynthetic capacity and prevent oxidative damage. However, the faster occurrence of metabolites content alterations in citral when compared to farnesene suggests that citral could be acting faster than farnesene in the *Arabidopsis* metabolism, which could also explain the stronger effect of citral on fluorescence parameters and the higher amounts of metabolites affected by citral in 24 h, which are reached by farnesene after 48 h of treatment.

The quicker toxic effect exerted by citral in comparison with farnesene can also be confirmed by observing the differential effects highlighted by the pathway analysis.

The comparison of 24 h citral treatment with 24 h farnesene treatment highlighted that among the 11 metabolic pathways with the highest impact, 5 routes were significantly affected by farnesene. In contrast, 8 routes were significantly affected by citral, demonstrating the ability of citral to alter the metabolism of early-treated seedlings quicker than farnesene. The routes altered by citral but not by farnesene were alanine aspartate and glutamate metabolism, citrate cycle (TCA cycle) and tryptophan metabolism.

For example, compounds belonging to the TCA cycle such as fumaric acid, pyruvic and citric acid significantly dropped down in citral treatment after 24 h. On the contrary, only fumaric and pyruvic acid in farnesene treatments were significantly inhibited after 48 h of treatment.

This alteration in the TCA cycle can affect the synthesis of amino acids such as aspartic acid (Lehmann et al., 2012; Savchenko and Tikhonov, 2021), thus altering the alanine, aspartate and glutamate metabolism, evidenced by the reduction in aspartate levels in 24 h citral treatment. This pathway is also affected by increased alanine levels, often elevated in stressful situations (Monselise, 2011). Miyashita and Good (2008) observed an accumulation of alanine in *A. thaliana* roots under hypoxia. Concerning tryptophan metabolism, Graña et al. (2013a) found that *A. thaliana* seedlings showed an increase in auxin content after 5 and 10 h of citral treatment, a phytohormone that can be biosynthesized in plants from

tryptophan (Morffy and Strader, 2020). After 48 h, the number of significantly altered pathways increases in both treatments. Considering the 11 altered pathways significantly impacted by the treatments, in the case of farnesene, there were 9 altered pathways while treatment with citral affected 10 pathways, with both treatments just differing in the tryptophan pathway, which was affected by citral but not by farnesene. This suggests a very similar behaviour in the mode of action of farnesene and citral in the treated seedlings. Whereas citral has been proven to alter the auxin balance in *Arabidopsis* seedlings (Graña et al., 2013), Araniti et al. (2017a) also demonstrated that farnesene-induced root growth alterations were mainly due to an altered distribution of auxin due to the inhibition of PIN proteins involved in auxin redistribution.

Focusing more on the effects, also the *in-silico* analysis highlighted similarities and differences between citral and farnesene. Graña et al. (2020) recently showed, through transcriptomic and *in silico* studies, that the mechanism of phytotoxicity of citral involves the interaction of citral isomers with single strand DNA binding proteins (SSBPs) inducing an almost total blockage of the plant metabolism in the first hours of citral treatment. Therefore, *in silico* molecular docking analysis was done in our study to compare citral and farnesene capacity to interact with SSBPs. *In silico* studies suggested binding of citral isomers and farnesene to the single strand DNA binding protein WHY2 and to other transcription factors such as ANAC, while not interesting interactions were observed for both compounds with WHY-1 and WHY-3. In fact, there is a clear similarity in the interaction of farnesene and citral with SSBPs, although also some differences were found in the mechanism of action of these two compounds. In particular, the main differences were related to the protein scarecrow (SCR) and MYC-2, located in root tissues, which were characterized by a higher affinity for citral (neral) than for farnesene, which could be related to the quicker action of citral in comparison with farnesene. For neral (citral), two hydrogen bonds with residues G584 and S583 were observed in the SHR-SCR-citral ICM docking and with L480 and S479 in the MYC-2-citral ICM docking in an energetically stabilized pose by the formation of a five-membered cycle, as indicated in a previous article (Graña et al., 2020), suggesting that these interactions could alter the binding of SCR-SHR and MYC-2 to ssDNA. However, these key interactions could not be observed in ICM docking studies between SHR-SCR and MYC-2 with farnesene. The ICM molecular docking models suggests that ligands binding sites for SCR and MYC-2 are located in different positions for neral and farnesene. While neral is located in a buried hydrophobic pocket, farnesene is located on the surface, in a water-exposed position. The low affinity of farnesene to SCR agrees with Araniti et al. (2017a), which demonstrated that *Arabidopsis* root treatment with this molecule (at the ED50 concentration) strongly affected PIN proteins but did not affect SCR distribution. The fast ability of the monoterpenoid

citral (C10, a much smaller molecule than farnesene) to enter in the DNA helix and interact with key positions of the DNA transcription can be the reason for the faster effect of citral on *Arabidopsis* (with an almost complete blockage of gene expression in the first minutes of treatment; Graña et al., 2020), when compared to the sesquiterpene farnesene (C15). Previous genotoxic studies have shown that disrupted DNA replication and transcription can affect genome stability, resulting in reduced protein synthesis, damage of cell membrane and photosynthetic proteins (Dutta et al., 2018), oxidative stress, and finally plant growth and development alterations, as shown for farnesene and citral.

Conclusions

Both metabolomic analysis and *in-silico* studies highlighted clear similarities in the metabolic pathways and metabolites profile affected by these two chemicals at different times but also differences concerning the affinity with the proteins with which they could potentially interact, suggesting a faster effect of citral when compared to farnesene but also the ability of citral to affect pathways (i.e. tryptophan route) not affected by farnesene. Those results suggest that the two molecules share many of the mechanisms of action on plant metabolism, especially those related to the immediate interaction with DNA binding proteins and the induction of oxidative stress, while the damage to the photosynthetic machinery could be a side effect due to a potential increase in ROS after both molecules' treatment. The apparent harmlessness of these compounds to other organisms together with their effect on plant metabolism make these compounds excellent candidates for further study of their mode of action in search of new natural molecules with potential herbicidal activity.

Acknowledgement

The MS was funded by the "Ministerio de Ciencia, Innovaciòn y Universidades" [grant code RTI2018-094716-B-100].

Data availability statement

The datasets generated during and/or analysed during the current study are available from the corresponding author on reasonable request.

Bibliography

Abagyan, R., Totrov, M., 1994. Biased probability Monte Carlo conformational searches and electrostatic calculations for peptides and proteins. J Mol Biol 235, 983–1002. https://doi.org/10.1006/jmbi.1994.1052.

Abagyan, R., Totrov, M., Kuznetsov, D., 1994. ICM-A New method for protein modeling and design: Applications to docking and structure prediction from the distorted native vonformation. J Comput Chem 15, 488–506. https://doi.org/https://doi.org/10.1002/jcc.540150503.

Aliferis, K.A., 2020. Metabolomics in plant protection product research and development: discovering the mode(s)-of-action and mechanisms of toxicity, in: Álvarez-Muñoz, D., Farré, M. (Eds.), Environmental Metabolomics Applications in Field and Laboratory Studies to Understand from Exposome to Metabolome. Elsevier, pp. 163–194.

Araniti, F., Costas-Gil, A., Cabeiras-Freijanes, L., Lupini, A., Sunseri, F., Reigosa, M. J., Abenavoli, M.R., Sanchez-Moreiras, A. M., 2018a. Rosmarinic acid induces programmed cell death in *Arabidopsis* seedlings through reactive oxygen species and mitochondrial dysfunction. PloS One, 13, e0208802. https://doi.org/10.1371/journal.pone.0208802.

Araniti, F., Bruno, L., Sunseri, F., Pacenza, M., Forgione, I., Bitonti, M.B., Abenavoli, M.R., 2017a. The allelochemical farnesene affects *Arabidopsis thaliana* root meristem altering auxin distribution. Plant Physiol. Biochem. 121, 14–20. https://doi.org/10.1016/j.plaphy.2017.10.005.

Araniti, F., Graña, E., Krasuska, U., Bogatek, R., Reigosa, M.J., Abenavoli, M.R., Sánchez-Moreiras, A.M., 2016. Loss of gravitropism in farnesene-treated arabidopsis is due to microtubule malformations related to hormonal and ROS unbalance. PLoS One 11, e0160202 . https://doi.org/10.1371/journal.pone.0160202.

Araniti, F., Graña, E., Reigosa, M.J., Sánchez-Moreiras, A.M., Abenavoli, M.R., 2013. Individual and joint activity of terpenoids, isolated from *Calamintha nepeta* extract, on *Arabidopsis thaliana*. Nat Prod Res 27, 2297–2303. https://doi.org/10.1080/14786419.2013.827193.

Araniti, F., Landi, M., Lupini, A., Sunseri, F., Guidi, L., Abenavoli, M. R., 2018b. *Origanum vulgare* essential oils inhibit glutamate and aspartate metabolism altering the photorespiratory pathway in *Arabidopsis thaliana* seedlings. J. Plant Physiol 231, 297–309. https://doi.org/10.1016/j.jplph.2018.10.006.

Araniti, F., Lupini, A., Sunseri, F., Abenavoli, M.R., 2017b. Allelopatic potential of *Dittrichia viscosa* (L.) W. Greuter mediated by VOCs: A physiological and metabolomic approach. PLoS One 12, e0170161. https://doi.org/10.1371/journal.pone.0170161.

Araniti, F., Miras-Moreno, B., Lucini, L., Landi, M., Abenavoli, M.R., 2020. Metabolomic, proteomic and physiological insights into the potential mode of action of thymol, a phytotoxic natural monoterpenoid phenol. Plant Physiology and Biochemistry 153, 141–153. https://doi.org/10.1016/j.plaphy.2020.05.008.

Formatted: English (United States)

Formatted: Italian (Italy)

Formatted: Italian (Italy)

Formatted: English (United States)

Formatted: Italian (Italy)

Formatted: Italian (Italy)

Formatted: Italian (Italy)

Baxter, C.J., Redestig, H., Schauer, N., Repsilber, D., Patil, K.R., Nielsen, J., Selbig, J., Liu, J., Fernie, A.R., Sweetlove, L.J., 2007. The metabolic response of heterotrophic *Arabidopsis* cells to oxidative stress. Plant Physiol 143, 312–325. https://doi.org/10.1104/pp.106.090431.

Bouché, N., Fromm, H., 2004. GABA in plants: Just a metabolite? Trends Plant Sci 9, 110–115. https://doi.org/10.1016/j.tplants.2004.01.006.

Bourguignon, J., Ribeilli, F., Douce, R., 1999. Serine and glycine metabolism in higher plants, in: Singh, B.K. (Ed.), Plant amino acids Biochemistry and Biotechnology. CRC Press, Boca Raton, pp. 111–146. https://doi.org/https://doi.org/10.1201/9781482270068.

Bresson, J., Vasseur, F., Dauzat, M., Koch, G., Granier, C., Vile, D., 2015. Quantifying spatial heterogeneity of chlorophyll fluorescence during plant growth and in response to water stress. Plant Methods 11, 1–15. https://doi.org/10.1186/s13007-015-0067-5.

Cappadocia, L., Parent, J.S., Sygusch, J., Brisson, N., 2013. A family portrait: Structural comparison of the Whirly proteins from *Arabidopsis thaliana* and *Solanum tuberosum*. Acta Crystallograph 69, 1207–1211. https://doi.org/10.1107/S1744309113028698.

Çelik, K., Toğar, B., Türkez, H., Taşpinar, N., 2014. In vitro cytotoxic, genotoxic, and oxidative effects of acyclic sesquiterpene farnesene. Turk J Biol 38, 253–259. https://doi.org/10.3906/biy-1309-55.

Chaimovitsh, D., Rogovoy Stelmakh, O., Altshuler, O., Belausov, E., Abu-Abied, M., Rubin, B., Sadot, E., Dudai, N., 2012. The relative effect of citral on mitotic microtubules in wheat roots and BY2 cells. Plant Biol 14, 354–364. https://doi.org/10.1111/j.1438-8677.2011.00511.x.

Duke, S., Pan, Z., Bajsa-Hirshel, J., Sánchez-Moreiras, A.M., Vaughn, J., 2018 Use of omics methods to determine the mode of action of natural phytotoxins, in: Beck, J. J., Rering, C. C., Duke, S. O., (Eds), Roles of Natural Products for Biorational Pesticides in Agriculture. ACS Symposium Series, pp. 33–46. doi: 10.1021/bk-2018-1294.ch005.

Duke, S.O., Dayan, F.E., 2022. The search for new herbicide mechanisms of action: Is there a 'holy grail'? Pest Manag Sci 78, 1303–1313. https://doi.org/10.1002/ps.6726.

Duke, S.O., Stidham, M.A., Dayan, F.E., 2019. A novel genomic approach to herbicide and herbicide mode of action discovery. Pest Manag Sci 75, 314–317. https://doi.org/10.1002/ps.5228.

Dutta S, Mitra M, Agarwal P, Mahapatra K, De S, Sett U, Roy S. 2018. Oxidative and genotoxic damages in plants in response to heavy metal stress and maintenance of genome stability. Plant Signal Behav 13, e1460048. doi: 10.1080/15592324.2018.1460048.

Formatted: English (United States)

Fagodia, S.K., Singh, H.P., Batish, D.R., Kohli, R.K., 2017. Phytotoxicity and cytotoxicity of *Citrus aurantiifolia* essential oil and its major constituents: Limonene and citral. Ind Crops Prod 108, 708–715. https://doi.org/10.1016/j.indcrop.2017.07.005.

Fernie, A.R., Carrari, F., Sweetlove, L.J., 2004. Respiratory metabolism: Glycolysis, the TCA cycle and mitochondrial electron transport. Curr Opin Plant Biol 7, 254–261. https://doi.org/10.1016/j.pbi.2004.03.007.

Gaines, T. A., Duke, S. O., Morran, S., Rigon, C. A., Tranel, P. J., Küpper, A., Dayan, F. E., 2020. Mechanisms of evolved herbicide resistance. J. Biol. Chem., 295, 10307–10330. https://doi.org/10.1074/jbc.REV120.013572.

Graña, E., Díaz-Tielas, C., Sánchez-Moreiras, A.M., Reigosa, M.J., Celeiro, M., Abagyan, R., Teijeira, M., Duke, M. v., Clerk, T., Pan, Z., Duke, S.O., 2020. Transcriptome and binding data indicate that citral inhibits single strand DNA-binding proteins. Physiol Plant 169, 99–109. https://doi.org/10.1111/ppl.13055.

Graña, E., Sotelo, T., Díaz-Tielas, C., Araniti, F., Krasuska, U., Bogatek, R., Reigosa, M.J., Sánchez-Moreiras, A.M., 2013a. Citral induces auxin and ethylene-mediated malformations and arrests cell division in *Arabidopsis thaliana* roots. J Chem Ecol 39, 271–282. https://doi.org/10.1007/s10886-013-0250-y.

Graña, Elisa, Sotelo, T., Díaz-Tielas, C., Reigosa, M.J., Sánchez-Moreiras, A.M., 2013b. The phytotoxic potential of the terpenoid citral on seedlings and adult plants. Weed Sci 61, 469–481. https://doi.org/10.1614/ws-d-12-00159.1.

Gressel, J., 2020. Perspective: present pesticide discovery paradigms promote the evolution of resistance–learn from nature and prioritize multi- target site inhibitor design. Pest Manag. Sci., 76, 421–425. https://doi.org/10.1002/ps.5649.

Hachisu, S., 2021. Strategies for discovering resistance-breaking, safe and sustainable commercial herbicides with novel modes of action and chemotypes. Pest Manag Sci 77, 3042–3048. https://doi.org/10.1002/ps.6397.

Ji, Y., Li, Q., Liu, G., Selvaraj, G., Zheng, Z., Zou, J., Wei, Y., 2019. Roles of cytosolic glutamine synthetases in *Arabidopsis* development and stress responses. Plant Cell Physiol 60, 657–671. https://doi.org/10.1093/pcp/pcy235.

Kavi Kishor, P.B., Sreenivasulu, N., 2014. Is proline accumulation per se correlated with stress tolerance or is proline homeostasis a more critical issue? Plant Cell Environ 37, 300–311. https://doi.org/10.1111/pce.12157.

Klughammer, C., Schreiber, U., 2008. Complementary PS II quantum yields calculated from simple fluorescence parameters measured by PAM fluorometry and the Saturation Pulse method. PAM Application Notes 1, 27–35.

Kramer, D.M., Johnson, G., Kiirats, O., Edwards, G.E., 2004. New fluorescence parameters for the determination of Q A redox state and excitation energy fluxes. Photosynth Res 79, 209–218. https://doi.org/https://doi.org/10.1023/B:PRES.0000015391.99477.0d.

Formatted: English (United States)

Formatted: English (United States)

Landi, M., Misra, B.B., Muto, A., Bruno, L., Araniti, F., 2020. Phytotoxicity, morphological, and metabolic effects of the sesquiterpenoid nerolidol on *Arabidopsis thaliana* seedling roots. Plants 9, 1–19. https://doi.org/10.3390/plants9101347.

López- González, D., Ledo, D., Cabeiras- Freijanes, L., Verdeguer, M., Reigosa, M.J., Sánchez- Moreiras, A.M., 2020. Phytotoxic activity of the natural compound norharmane on crops, weeds and model plants. Plants 9, 1–23. https://doi.org/10.3390/plants9101328.

Martínez-Peñalver, A., Reigosa, M.J., Sánchez-Moreiras, A.M., 2011. Imaging chlorophyll *a* fluorescence reveals specific spatial distributions under different stress conditions. Flora: Morphology, Distribution, Functional Ecology of Plants 206, 836–844. https://doi.org/10.1016/j.flora.2011.02.004.

Oikonomou, A., Ladikou, E.V., Chatziperou, G., Margaritopoulou, T., Landi, M., Sotiropoulos, T., Araniti, F., Papadakis, I.E., 2019. Boron excess imbalances root/shoot allometry, photosynthetic and chlorophyll fluorescence parameters and sugar metabolism in apple plants. Agronomy 9, 1–17. https://doi.org/10.3390/agronomy9110731.

Osei- Bonsu, I., McClain, A. M., Walker, B. J., Sharkey, T. D., Kramer, D. M., 2021. The roles of photorespiration and alternative electron acceptors in the responses of photosynthesis to elevated temperatures in cowpea. Plant Cell Environ., 44, 2290–2307. https://doi.org/10.1111/pce.14026.

Podlešáková, K., Ugena, L., Spíchal, L., Doležal, K., de Diego, N., 2019. Phytohormones and polyamines regulate plant stress responses by altering GABA pathway. N Biotechnol 48, 53–65. https://doi.org/10.1016/j.nbt.2018.07.003.

Sánchez-Moreiras, A.M., Graña, E., Reigosa, M.J., Araniti, F., 2020. Imaging of chlorophyll *a* fluorescence in natural compound-induced stress detection. Front Plant Sci 11, 583590. https://doi.org/10.3389/fpls.2020.583590.

Schapira M, Totrov M, Abagyan R (1999) Prediction of the binding energy for small molecules, peptides and proteins J Mol Recognit 12, 177–190. https://doi.org/10.1002/(SICI)1099-1352(199905/06)12:3<177::AID-JMR451>3.0.CO;2-Z.

Szabados, L., Savouré, A., 2010. Proline: a multifunctional amino acid. Trends Plant Sci 15, 89–97. https://doi.org/10.1016/j.tplants.2009.11.009.

Trenkamp, S., Eckes, P., Busch, M., Fernie, A.R., 2009. Temporally resolved GC-MS-based metabolic profiling of herbicide treated plants treated reveals that changes in polar primary metabolites alone can distinguish herbicides of differing mode of action. Metabolomics 5, 277–291. https://doi.org/10.1007/s11306-008-0149-8.

Ünlüsoy, A. G., Yolcu, S., Bor, M., Özdemir, F., Türkan, İ., 2022. Activation of photorespiration facilitates drought stress tolerance in *Lotus corniculatus*. J. Plant Growth Regul., 1–14. https://doi.org/10.1007/s00344-022-10683-5.

Vaughn, S.F., Spencer, G.F., 1993. Volatile monoterpenes as potential parent structures for new herbicides. Weed Sci 41, 114–119. https://doi.org/10.1017/S0043174500057672.

Verdeguer, M., Sánchez-Moreiras, A.M., Araniti, F., 2020. Phytotoxic effects and mechanism of action of essential oils and terpenoids. Plants 9, 1–52. https://doi.org/10.3390/plants9111571.

Vuorinen, T., Reddy, G.V.P., Nerg, A.M., Holopainen, J.K., 2004. Monoterpene and herbivore-induced emissions from cabbage plants grown at elevated atmospheric CO_2 concentration. Atmos Environ 38, 675–682. https://doi.org/10.1016/j.atmosenv.2003.10.029.

Waters, E.R., Lee, G.J., Vierling, E., 1996. Evolution, structure and function of the small heat shock proteins in plants. J Exp Bot 47, 325–338. https://doi.org/https://doi.org/10.1093/jxb/47.3.325.

Witte, C. P., 2011. Urea metabolism in plants. Plant Sci, 180, 431–438. https://doi.org/10.1016/j.plantsci.2010.11.01.

Xia, J., Sinelnikov, I. v., Han, B., Wishart, D.S., 2015. MetaboAnalyst 3.0-making metabolomics more meaningful. Nucleic Acids Res 43, W251–W257. https://doi.org/10.1093/nar/gkv380.

Authors contribution

Conceptualization: AF, SMAM; *Data curation:* AF, SMAM, TM, VM, RMJ, LGD, GE; *Formal analysis:* AF, TM, LGD, GE; *Funding acquisition:* SMAM; AF, VM, TM; *Investigation:* AF, SMAM; *Data curation:* AF, SMAM, TM, VM, RMJ, LGD, GE**;** *Methodology:* AF, SMAM; *Data curation:* AF, SMAM, TM, VM, RMJ, LGD, GE**;** *Project administration:* SMAM; *Supervision:* AF, SMAM, TM, VM, RMJ; *Validation:* LGD, GE**;** *Visualization:* AF, SMAM, TM, VM, RMJ**;** *Writing - review & editing:* AF, SMAM, TM, VM, RMJ, LGD, GE.

Supplementary material Table S1

Authors statement

On behalf of the authors, I declare that none of the materials in this manuscript have been published or are concurrently submitted elsewhere. Also, the authors have no competing interests to declare.